JACS
JOURNAL OF THE AMERICAN CHEMICAL SOCIETY

Article

pubs.acs.org/JACS

Directing the Crystallization of Dehydro[24]annulenes into Supramolecular Nanotubular Scaffolds

Mitsuharu Suzuki,[†] Juliet F. Khosrowabadi Kotyk, Saeed I. Khan, and Yves Rubin*

Department of Chemistry and Biochemistry, University of California, Los Angeles, 607 Charles E. Young Drive East, Los Angeles, California 90095, United States

Supporting Information

ABSTRACT: The self-assembly of a series of dehydro[24]-annulene derivatives into columnar stacks has been examined for its latent ability to form π-conjugated carbon-rich nanotubular structures through topochemical polymerizations. We have studied the parameters affecting self-assembly, including the nature of the substituent and crystallization conditions, using 10 different dehydro[24]annulene derivatives. In particular, hydrogen-bonding interactions through carbamate groups were found to be especially useful at directing the formation of nanotubular supramolecular assemblies. We have also evaluated the electronic coupling between neighboring dehydroannulene molecules within these supramolecular assemblies. Density functional calculations on the stacked supramolecular nanotube assemblies show that transfer integrals vary considerably between the three columnar assemblies, ranging from moderate to high (59−98 meV for the highest occupied molecular orbitals, 63−97 meV for the lowest unoccupied molecular orbitals), depending on the local molecular topology. In addition, the dehydro[24]annulene derivatives afforded distinct architectures in the crystal, including nanochannel arrays, sheets with solvent-filled pores, and lamellae. This work is an essential step toward a controlled formation of covalently linked carbon-rich nanostructures generated from molecular precursors with a latent diacetylene reactivity.

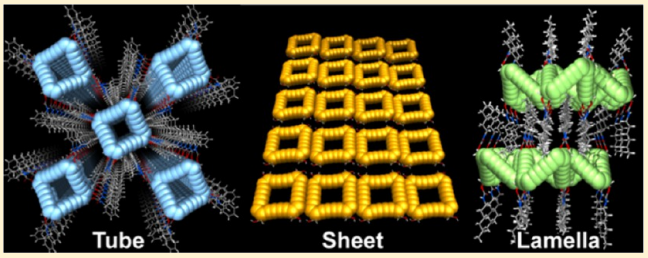

INTRODUCTION

The chemical and physical properties of organic molecules can be closely correlated with their packing arrangement in the crystalline state. In particular, several chemical reactions have been investigated on the basis of the topochemical principle, in which the course and outcome of a reaction are primarily defined by the solid-state arrangement of the reactants.[1−7] The electronic and optoelectronic characteristics of molecular semiconductors are also strongly affected by the solid-state packing and morphology of individual molecules, making these considerations directly relevant to the performance of organic devices such as field-effect transistors and photovoltaic devices.[8−17] Accordingly, much research has been devoted to understanding how intermolecular interactions dictate molecular packing, and how these interactions can be engineered into molecular solids for their intended applications.[18]

We have been working on such a molecular engineering approach to supramolecular architectures based on dehydroannulenes,[19] a class of compounds with a carbon-rich π-conjugated macrocycle containing several diacetylene units. We chose the dehydroannulenes because of the inherently high kinetic strain contained in their diacetylenic carbons, which are prone to expand their coordination. Along this line, the pioneering results by the groups of Vollhardt[20,21] and Bunz[22] have shown that dehydroannulenes can produce carbon nanotubes and carbon onions in explosive, high-temperature, solid-state reactions. Although these reactions afforded a messy mixture of structures, we envisioned that an exquisitely controlled solid-state reaction of dehydroannulenes using the topochemical polymerization principle would give a pristine polymeric structure resulting from the highly organized state of molecules within a crystal and the minimal amount of atomic movement in most topochemical polymerizations.[7,23−32] Scheme 1 shows the potential of this approach, in which dehydro[24]annulene macrocycles are stacked in a crystal to form nanotubular assemblies. If these assemblies fulfill the required packing parameters for a four-fold butadiyne topochemical polymerization, it could occur on all four sides of the molecule. The ensuing product would be a fully π-conjugated carbon-rich nanotubular structure having a distinct framework topology.

The topochemical polymerization of butadiynes has been extensively studied, and thus, the principles of molecular design and reaction conditions for forming poly(butadiyne)s are well established.[7,23−33] In fact, the butadiyne topochemical polymerization has not been limited to simple, linear substrates, but also also been extended to macrocyclic systems.[25,34−41] However, the use of *dehydroannulenes* as monomers in topochemical polymerization remains a significant challenge, even though this concept has been invoked in several reports.[42−48] Only one successful example has been reported so far, in which a

Received: February 21, 2016
Published: April 18, 2016

DOI: 10.1021/jacs.6b01939
J. Am. Chem. Soc. 2016, 138, 5939−5956

Scheme 1. Four-fold Topochemical Polymerization of a Dehydro[24]annulene[a]

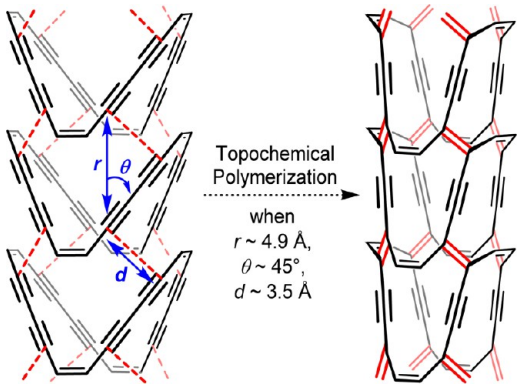

[a]A columnar assembly of dehydro[24]annulene molecules that can potentially undergo the butadiyne-to-polydiacetylene topochemical polymerization at each of the four macrocycle edges (left, the reaction pathway is indicated by red dashed lines), providing a π-conjugated nanotubular scaffold (right, newly formed covalent C═C bonds shown in red). Ideal packing parameters for the butadiyne topochemical polymerization are repeat distance r = 4.9 Å, tilt angle θ = 45°, and C1···C4′ distance d = 3.5 Å. Note that small deviations from these values are acceptable for topochemical polymerization.

Chart 1. Structures of Dehydro[24]annulene Derivatives 1a−1j

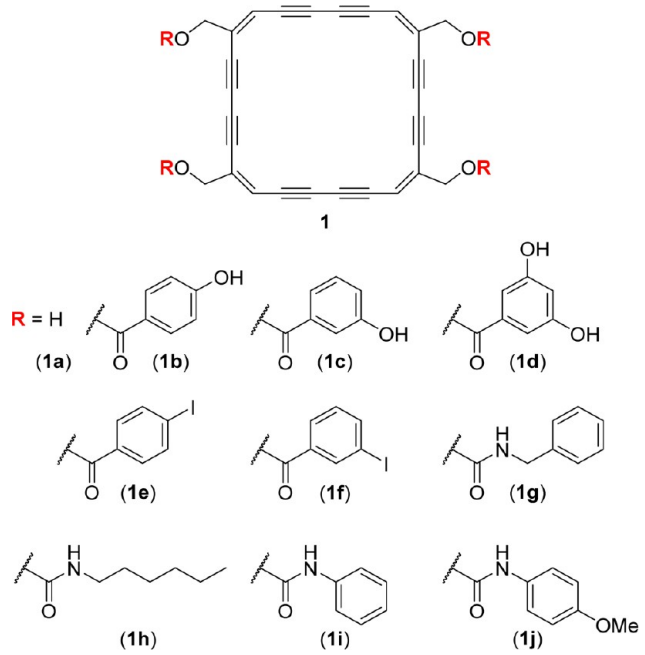

tribenzodehydro[14]annulene was polymerized in the single-crystalline state under high-pressure conditions.[49] The scarcity of controlled polymerization of dehydroannulenes appears to be due, in part, to the general instability of these compounds in the solid state. Indeed, dehydroannulenes are largely underrepresented in the field of crystal engineering. The systematic investigation of their solid-state packing is limited to a few rigid and relatively stable systems such as benzo-fused dehydro[12]annulenes.[43−47,50−52] For conformationally flexible derivatives not endowed with stabilizing benzoannulation, crystallographic characterization of molecular structures has been rather elusive.[53] Furthermore, the weak intermolecular $\pi-\pi$ interactions between acetylene units do not promote the formation of face-to-face stacks of dehydroannulenes.[54] Consequently, tubular assemblies based on flexible, non-benzoannulated dehydroannulenes are absent in the literature.

We are reporting here an extensive crystal-engineering study on a series of the tetrasubstituted dehydro[24]annulenes **1a−1j** (Chart 1). By employing directional non-covalent interactions, we have achieved nanotubular assemblies that possess near-ideal packing parameters for the four-fold topochemical polymerization described in Scheme 1. We have also accessed a variety of other dehydro[24]annulene-based supramolecular architectures through modification of the substituents and the crystallization conditions. In addition, we have evaluated the electronic coupling between neighboring dehydroannulene molecules within the obtained supramolecular nanotubes. Density-functional calculations show that the transfer integrals range from moderate to high for both the highest occupied molecular orbitals (HOMOs) and the lowest unoccupied molecular orbitals (LUMOs), depending on the local arrangement of molecules, confirming that there is a significant degree of interaction between the dehydroannulene units in these stacks. Overall, our experimental findings constitute an important first step in the exploration of the chemical and physical properties of rigid molecular solids constructed from dehydroannulenes.

RESULTS AND DISCUSSION

Molecular Design. Among a wide variety of conceivable dehydroannulene structures for the aim of this project (Scheme 1), dehydro[24]annulene **1** incorporating four butadiyne units (Chart 1) was chosen as the best test system because of its folded conformation and relatively high synthetic accessibility. As reported in our preliminary communication,[19] four-fold substitution with small polar groups such as hydroxymethyl (**1a**) considerably improves the solid-state stability of the otherwise highly reactive dehydro[24]annulene framework.[55] Benzoannulation was avoided even though this motif is highly effective at stabilizing dehydroannulenes. The steric encumbrance of benzene rings adjacent to butadiyne units has been known to impede topochemical polymerization.[56,57] To facilitate self-association in the crystal, all the dehydro[24]annulene substituents in compounds **1a−1j** were endowed with either hydrogen- or halogen-bonding functionalities so that highly organized molecular packing motifs could be gained through directional non-covalent interactions. The methylene "hinge" between each functional group and the dehydro[24]annulene framework was expected to allow a good degree of conformational flexibility to assist self-association processes, as well as to accommodate structural changes during the topochemical polymerization reactions in the solid state.

Conformational Flexibility of the Dehydro[24]annulene Framework and Pseudopolymorphism. Diffraction parameters and crystal data for all the crystal structures discussed in this paper are presented in Table 1. Tetraol **1a**, the simplest derivative in the series, provided different packing motifs depending on the solvent system employed for crystallization. While all the dehydro[24]annulene derivatives **1a−1j** are pale yellow in solution, red plates were obtained when **1a** was crystallized by slow diffusion of a small, linear or oblong-shaped solvent (MeOH, MeCN, or CH_2Cl_2) into a THF solution. Single-crystal X-ray diffraction analysis revealed that the dehydro[24]annulene framework in these red crystals adopts an unusual planar conformation, resulting in the

DOI: 10.1021/jacs.6b01939
J. Am. Chem. Soc. 2016, 138, 5939−5956

Table 1. Single-Crystal X-ray Diffraction Parameters and Crystal Data

	1a-I	1a-II	1a-III	1b	1c	1d	1f
formula	$C_{28}H_{16}O_4 \cdot CH_2Cl_2$	$C_{28}H_{16}O_4 \cdot (C_4H_{10}O)_2$	$C_{28}H_{16}O_4 \cdot C_3H_6O$	$C_{56}H_{32}O_{12} \cdot (C_4H_8O)_5$	$C_{56}H_{32}O_{12} \cdot (CH_2Cl_2)_3$	$C_{56}H_{32}O_{16} \cdot (C_3H_6O)_3$	$C_{56}H_{28}I_4O_8$
formula weight	501.33	564.65	474.49	1257.34	1151.59	1135.05	1336.38
crystal system	triclinic	triclinic	monoclinic	triclinic	triclinic	triclinic	triclinic
space group	$P\bar{1}$	$P\bar{1}$	$P2_1/n$	$P\bar{1}$	$P\bar{1}$	$P\bar{1}$	$P\bar{1}$
a (Å)	7.127(2)	8.6953(14)	16.538(10)	9.613(5)	7.8633(11)	8.0494(17)	9.2751(14)
b (Å)	7.465(2)	8.8490(14)	6.995(4)	13.191(7)	12.4758(18)	12.367(3)	11.8804(18)
c (Å)	11.374(4)	20.955(3)	22.907(14)	13.847(7)	14.475(2)	14.371(3)	13.115(2)
α (deg)	96.247(3)	83.764(2)	90	70.530(6)	87.013(2)	87.308(2)	103.213(2)
β (deg)	90.085(4)	81.190(2)	106.113(6)	89.281(6)	79.310(2)	76.651(2)	104.214(2)
γ (deg)	100.706(4)	89.372(2)	90	79.425(6)	78.040(2)	77.200(3)	112.564(1)
V (Å^3)	590.9(3)	1583.9(4)	2546(3)	1625.2(14)	1364.9(3)	1357.3(5)	1206.6(3)
Z	1	2	4	1	1	1	1
T (K)	100(2)	100(2)	100(2)	100(2)	100(2)	100(2)	100(2)
crystal description	red plate	red block	yellow block	red prism	red plate	red plate	red plate
crystal size (mm^3)	0.25 × 0.15 × 0.10	0.15 × 0.05 × 0.05	0.30 × 0.10 × 0.05	0.20 × 0.10 × 0.05	0.40 × 0.30 × 0.05	0.35 × 0.20 × 0.10	0.20 × 0.10 × 0.04
$2\theta_{min}$, $2\theta_{max}$ (deg)	7.90, 58.42	7.82, 56.58	7.64, 58.56	7.40, 57.21	7.80, 58.24	7.22, 58.04	7.46, 56.66
no. of reflns (unique)	3103	7663	6909	8025	7115	6995	5867
no. of reflns ($I > 2\sigma(I)$)	2760	4530	4852	4873	5008	5093	5092
$R1$, $wR2$ (all data)	0.0518, 0.1268	0.1194, 0.2063	0.0741, 0.1172	0.1067, 0.1677	0.1065, 0.2109	0.0914, 0.1938	0.0294, 0.0573
R, wR ($I > 2\sigma(I)$)	0.0466, 0.1224	0.0673, 0.1776	0.0458, 0.1050	0.0585, 0.1411	0.0770, 0.1910	0.0662, 0.1765	0.0232, 0.0542
GOF on F^2	1.044	1.034	1.028	1.013	1.114	1.086	1.026
Δ, e Å^{-3}	0.818, −0.569	0.367, −0.233	0.248, −0.292	0.589, −0.360	1.009, −0.606	0.537, −0.593	0.780, −0.392

	1b·2b[a]	1a·2a	1g-I[a]	1g-II[a]	1h	1i[a]	1j
formula	$C_{56}H_{32}O_{12} \cdot C_{14}H_{14}N_4O_2$	$C_{28}H_{16}O_4 \cdot C_{14}H_{14}N_4O_2$	$C_{60}H_{44}N_4O_8$	$C_{60}H_{44}N_4O_8 \cdot (C_4H_8O)_2$	$C_{56}H_{68}N_4O_8$	$C_{56}H_{36}N_4O_8$	$C_{60}H_{44}N_4O_{12} \cdot (C_3H_6O)_4$
formula weight	1167.11	686.70	948.99	1093.20	925.14	892.89	1245.30
crystal system	monoclinic	triclinic	monoclinic	orthorhombic	triclinic	tetragonal	triclinic
space group	$C2/c$	$P\bar{1}$	$C2$	$Pca2_1$	$P\bar{1}$	$I\bar{4}$	$P\bar{1}$
a (Å)	38.92(2)	8.896(3)	21.686(9)	9.9571(10)	10.0954(13)	25.112(7)	10.2111(8)
b (Å)	4.918(3)	9.089(3)	4.784(2)	17.4414(19)	16.195(2)	25.112(7)	10.4183(8)
c (Å)	38.53(2)	10.731(4)	27.556(13)	42.952(5)	16.930(2)	8.489(3)	16.0100(12)
α(deg)	90	88.821(4)	90	90	105.474(2)	90	78.912(1)
β (deg)	101.655(12)	89.682(5)	102.913(10)	90	95.831(2)	90	83.712(1)
γ(deg)	90	85.649(4)	90	90	91.576(2)	90	72.751(1)
V (Å^3)	7224(7)	865.0(5)	2786(2)	7459.3(14)	2649.5(6)	5353(3)	1593.7(2)
Z	4	1	2	4	2	4	1
T (K)	100(2)	100(2)	100(2)	100(2)	100(2)	100(2)	100(2)
crystal description	yellow needle	red block	yellow needle	yellow block	yellow block	yellow needle	red prism
crystal size (mm^3)	0.60 × 0.20 × 0.05	0.25 × 0.20 × 0.15	0.40 × 0.25 × 0.05	0.50 × 0.35 × 0.15	0.40 × 0.30 × 0.05	0.35 × 0.10 × 0.10	0.50 × 0.30 × 0.15
$2\theta_{min}$, $2\theta_{max}$ (deg)	8.14, 57.06	7.60, 57.64	7.52, 56.72	7.82, 58.22	7.54, 56.56	7.56, 56.94	7.80, 58.18
no. of reflns (unique)	9096	4377	3820	19972	12848	3593	8275
no. of reflns ($I > 2\sigma(I)$)	5366	3863	2705	14515	8008	2184	6862
$R1$, $wR2$ (all data)	0.1166, 0.2056	0.0432, 0.1019	0.0994, 0.2067	0.0935, 0.2147	0.1279, 0.2157	0.1078, 0.1738	0.0499, 0.1058
R, wR ($I > 2\sigma(I)$)	0.0729, 0.1852	0.0381, 0.0982	0.0754, 0.1932	0.0718, 0.2008	0.0764, 0.1951	0.0637, 0.1556	0.0396, 0.0991
GOF on F^2	0.962	1.018	1.040	1.037	1.094	1.073	1.027
Δ, e Å^{-3}	0.291, −0.277	0.453, −0.244	0.254, −0.216	0.490, −0.320	0.344, −0.297	0.258, −0.212	0.377, −0.187

[a]The disordered solvent molecules could not be properly refined, and the corresponding diffused electron density was treated with the SQUEEZE routine of the PLATON program.

formation of an array of solvent-accessible channels, each of which is walled by highly polarizable π electrons in the diacetylene units (Figure 1).

As the packing motifs are essentially the same for **1a** crystallized from all three solvent systems (THF with MeOH, MeCN, or CH_2Cl_2), only the pseudopolymorph containing CH_2Cl_2 (referred to as **1a-I**) is described here. The planarized macrocyclic framework in **1a-I** has nonequivalent minimum distances for the two sets of mutually opposed edges, indicating a strong distortion due to crystal packing effects: i.e., 7.546(3)

DOI: 10.1021/jacs.6b01939
J. Am. Chem. Soc. 2016, 138, 5939−5956

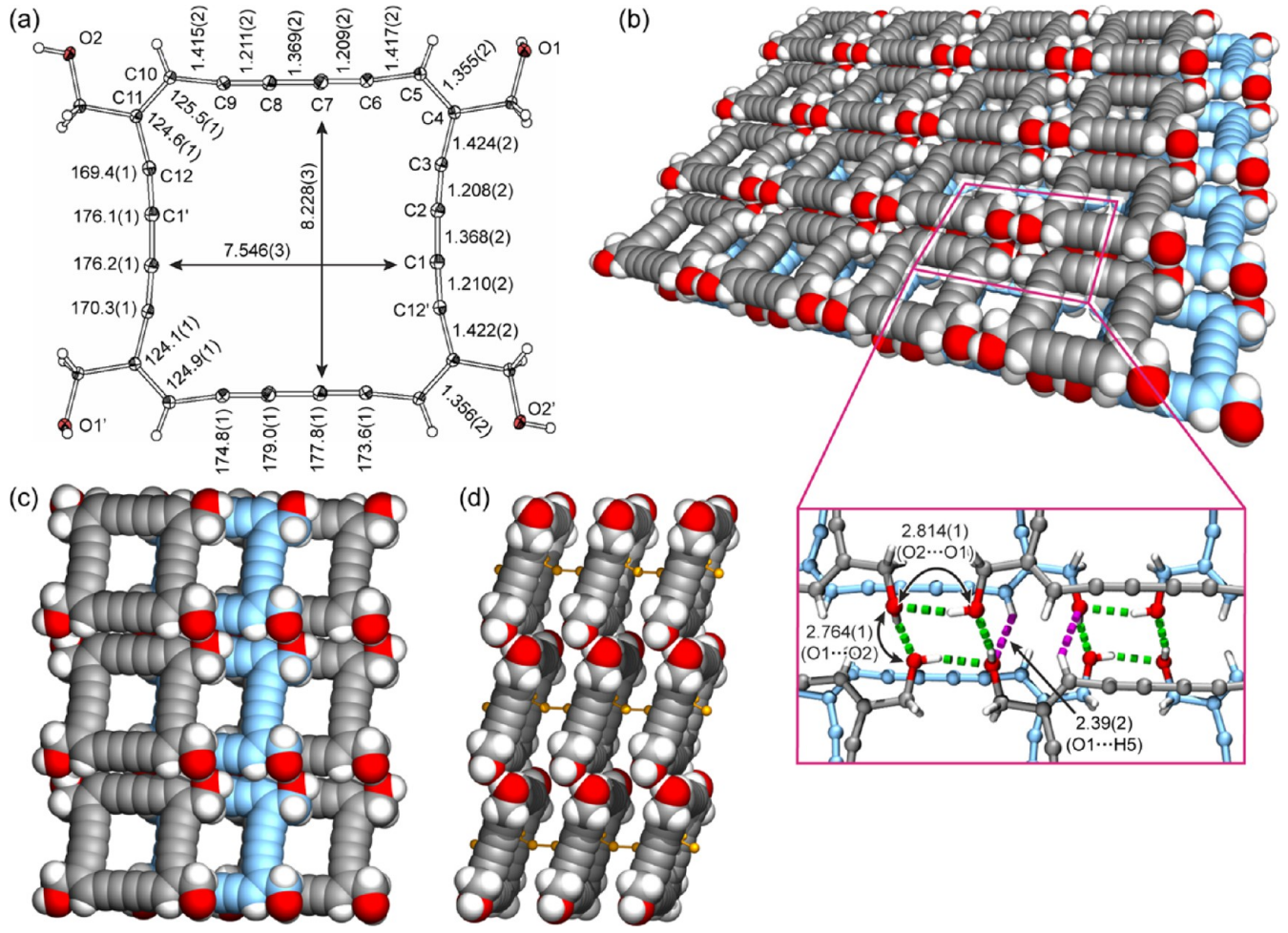

Figure 1. Representations of the pseudopolymorph **1a-I**. Selected bond angles and interatomic distances are given in degrees and angstroms, respectively. (a) Thermal ellipsoid plot of tetraol **1a** at 50% probability. (b) Sheet motif observed in **1a-I**. Inset: Close-up view highlighting the intrasheet tetragonal hydroxy hydrogen-bonding motif (green dashed lines) and intersheet C(sp^2)–H···O interactions (magenta dashed lines). (c,d) Molecular packing in **1a-I** viewed along and perpendicular to the nanochannel axis, respectively. Disordered solvent molecules (CH_2Cl_2) within the channels are omitted for clarity in (c), whereas they are shown as yellow ball-and-stick models in (d).

Å for C1···C2′ and 8.228(3) Å for C7···C8′ (Figure 1a). The Cl–C–Cl planes of the occluded CH_2Cl_2 molecules are approximately parallel to the longer edge-to-edge axis. All four hydroxy groups of each macrocycle are engaged in intermolecular hydrogen bonds with a cyclic tetragonal motif, which results in the formation of a corrugated sheet structure comprising the dehydro[24]annulene frameworks (Figure 1b). The corresponding intermolecular O1···O2 distances of 2.814(1) and 2.764(1) Å are typical values for hydrogen bonds between aliphatic alcohols.[58] The corrugated sheets stack on top of each other, mediated by short C(sp^2)–H···O contacts of 2.39(2) Å (H5···O2, Figure 1b) as well as C(sp^2)···C(sp) contacts of 3.389(2) Å (C4···C9, see Supporting Information (SI)).

The nanochannel array obtained here is reminiscent of the organic crystal with wide channels reported by Moore et al.[59] The authors showed that a phenolic derivative of a hexagonally shaped *m*-phenylene-ethynylene macrocycle formed extended porous sheets in which the associated hydrogen-bonding motif could be described as an $R_3^3(33)$ graph set according to Etter's terminology.[60] The sheets stacked with a proper registry to construct solvent-accessible channels with ca. 9 Å in diameter. The authors attributed the observed inter-sheet alignment to π–π stacking interactions between the aromatic rings. In the present case of our system **1a-I**, the square-shaped tetraol forms a much "denser" hydrogen-bonding motif of four hydroxy groups that can be described as an $R_4^4(8)$ graph set, and the resulting sheet structure is not flat but corrugated. The corrugation is probably present to accommodate optimal hydrogen-bonding interactions with minimal angle strain. The π–π interactions between dehydroannulene frameworks are weak[54] and are likely less responsible for the observed intersheet registry as compared to other factors such as effective solvent inclusion and the formation of the C(sp^2)–H···O contacts.

A different pseudopolymorph **1a-II** was obtained by slow diffusion of Et_2O into a THF solution of **1a** (Figure 2). In this case, the unit cell consists of two symmetry-independent planarized macrocycles and two disordered Et_2O molecules. The two macrocycles are referred to as **1a-II(A)** and **1a-II(B)** and differentiated by gray and light blue colors, respectively (Figure 2). Inspection of the extended crystal structure reveals channel-like structures based on the macrocyclic frameworks (Figure 2c). However, in contrast to the case of pseudopolymorph **1a-I**, the solvent molecules in **1a-II** are sandwiched between two macrocycles rather than aligned along the channel

DOI: 10.1021/jacs.6b01939
J. Am. Chem. Soc. 2016, 138, 5939–5956

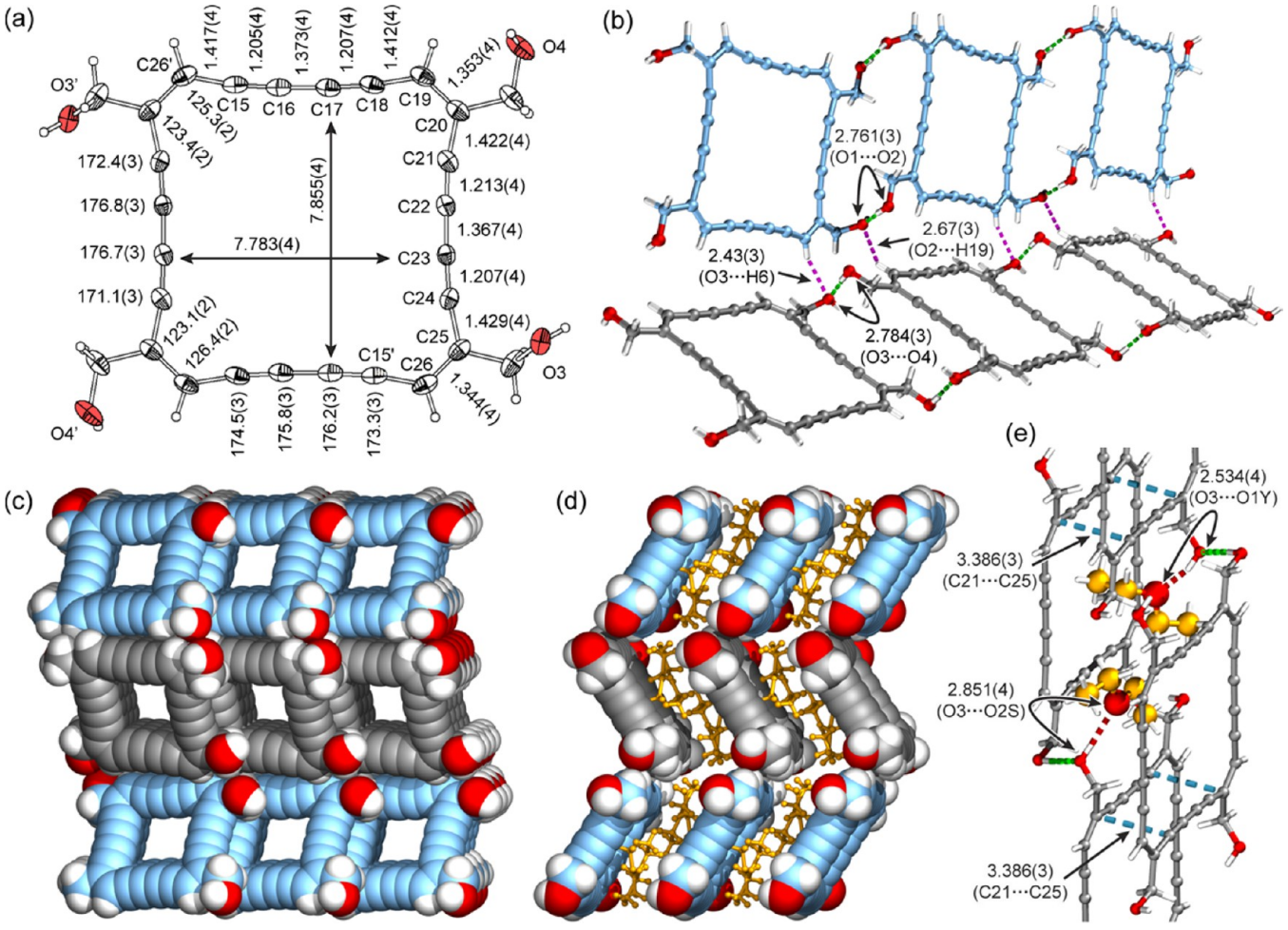

Figure 2. Representations of pseudopolymorph **1a-II**. Selected bond angles and interatomic distances are given in degrees and angstroms, respectively. (a) Thermal ellipsoid plot of molecule **1a-II(A)** at 50% probability. (b) Ladder motif observed in **1a-II**. Carbon atoms are gray for **1a-II(A)**, and blue for **1a-II(B)**. Hydroxy−hydroxy and C(sp^2)−H···O interactions are indicated with green and magenta dashed lines, respectively. (c, d) Molecular packing in **1a-II** along and perpendicular to the pseudochannel structures, respectively. Disordered solvent molecules are omitted for clarity in (c), while they are shown as yellow ball-and-stick models in (d). (e) Close-up view highlighting the sandwiched Et_2O molecules and intermacrocyclic short contacts (light blue dashed lines) in **1a-II(A)**. The interactions between the hydroxy groups of **1a-II(A)** and the oxygen atoms of Et_2O are indicated with red dashed lines. Each Et_2O molecule is disordered adopting two different conformations with a 50:50 probability, and only one conformation for each is shown for clarity.

axis (Figure 2d,e). Thus, the motif in the latter structure would be better described as a "pseudochannel". Several intermolecular interactions are observed between neighboring molecules of **1a**: The hydroxy−hydroxy interactions afford 1D extended ladder structures (Figure 2b, green dashed lines), which can be described as an $R_2^2(22)$ graph set. All the remaining hydroxy hydrogen atoms interact with the oxygen atoms of Et_2O (Figure 2e, red dashed lines for **1a-II(A)**; see SI for **1a-II(B)**). Consequently, there are no hydroxy hydrogen bonds between neighboring ladder structures, and instead, C(sp^2)−H···O contacts are present (Figure 2b, magenta dashed lines). The closest intermacrocyclic C···C contacts are found between C21 and C25 of **1a-II(A)** with a distance of 3.386(3) Å (Figure 2e, light blue dashed lines).

The longitudinal and lateral edge-to-edge distances of each macrocyclic framework in **1a-II** are very similar (7.783(4) and 7.855(4) Å for **1a-II(A)**, 7.826(4) and 7.842(3) Å for **1a-II(B)**), in clear contrast to the case of **1a-I** (Figures 1a and 2a). In connection with this observation, a DFT calculation predicts that the edge-to-edge distances are essentially the same between the two orthogonal directions (7.881 and 7.913 Å) for the planarized macrocyclic framework of **1a** in the gas phase (Figure S51 in SI).[61] Additionally, numerous short contacts are observed between solvent molecules (CH_2Cl_2) and the inner wall of macrocyclic frameworks in **1a-I**, all of which are along the longer edge-to-edge axis of the framework. Based on these observations, it is presumed that the macrocycles in **1a-I** are distorted to accommodate the CH_2Cl_2 molecules within the inner cavity.[62] In the case of **1a-II**, the solvent Et_2O is sterically more demanding and cannot fit within the macrocyclic cavity; thus, the solvents are sandwiched instead. In other words, the formation of these two different pseudopolymorphs may be primarily attributed to the differences in physical dimension of the occluded solvents.

The third type of pseudopolymorph of tetraol **1a** (**1a-III**) was obtained using a "branched" solvent. Single crystals grown from a heterogeneous solid−liquid mixture of compound **1a** and acetone are light yellow and block-shaped. Their appearance is in sharp contrast to those of pseudopolymorphs **1a-I** and **1a-II**, which are both obtained as red plates. X-ray diffraction analysis revealed that pseudopolymorph **1a-III** has **1a**·$(CH_3)_2CO$ stoichiometry, and the macrocyclic framework of

DOI: 10.1021/jacs.6b01939
J. Am. Chem. Soc. 2016, 138, 5939−5956

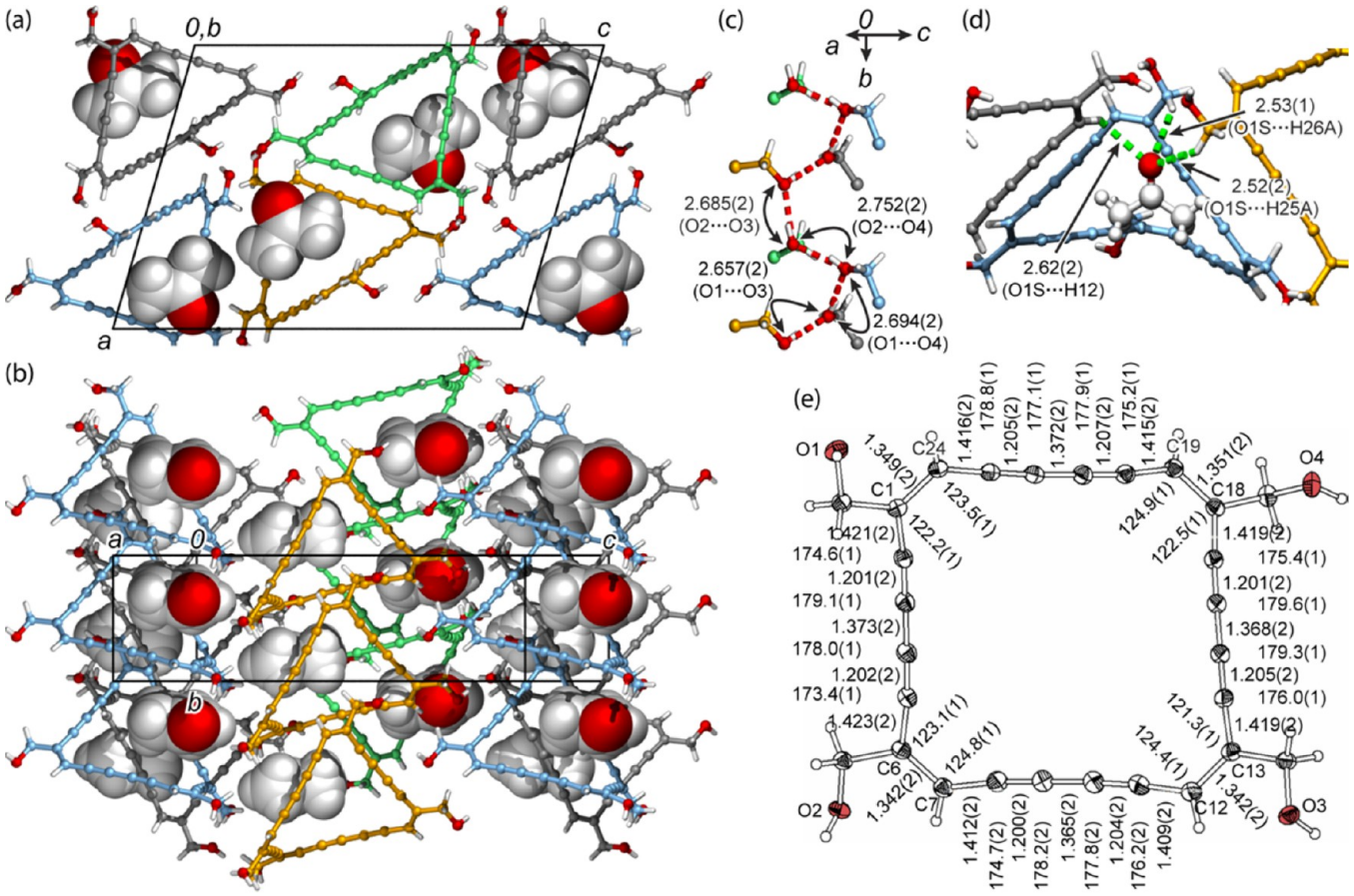

Figure 3. Representations of pseudopolymorph **1a-III**. Selected bond angles and interatomic distances are given in degrees and angstroms, respectively. (a,b) Packing diagrams along and perpendicular to the *b* axis, respectively. (c) Close-up view of the 1D extended hydroxy hydrogen-bonding network (red dashed lines) (d) Close-up view highlighting the three C(sp^2)–H···O interactions associated with an acetone oxygen atom (green dashed lines). (e) Thermal ellipsoid plot of **1a** at 50% probability.

tetraol **1a** adopts a folded conformation (Figure 3). All the hydroxy groups are engaged in intermolecular hydroxy–hydroxy interactions to form a helical motif along the *b* axis (Figure 3c). The associated O···O distances (2.657(2)–2.752(2) Å) are slightly shorter than those observed in **1a-I** or **1a-II**, probably reflecting the higher degree of polarization-enhancement effect in the extended chain motif.[58,63,64] Each acetone molecule sits in the middle of a dehydro[24]annulene framework (Figure 3a,b) without forming any hydroxy hydrogen bonds; instead, the acetone oxygen is in contact with three C–H hydrogen atoms from two methylene groups and one C(sp^2)–H unit of **1a** (Figure 3d).

Two of the three pseudopolymorphs of tetraol **1a** involve planar dehydro[24]annulene frameworks, which are conformationally strained and formally antiaromatic. The observed near-perfect planarity is unusual in that the planarization is achieved without any conformational constraints via covalent bonds, e.g., small-ring annulation[65,66] or inter-annular bridging.[67] At the same time, this observation is reasonable if one considers the fact that the energy required to planarize the macrocyclic framework from the most stable nonplanar conformation is estimated to be less than 4 kcal mol^{-1} in the gas phase by DFT calculations (Table S1, SI). The small enthalpy requirement is easily compensated by stabilizing non-covalent interactions in the crystalline state, such as hydrogen-bonding and van der Waals interactions. The conformational strain associated with the planarization is manifested by the differences in bond angles between the macrocyclic frameworks in **1a-II** and **1a-III** (Figures 2a and 3e). The smallest difference is observed for the substituted sp^2 carbons (0.7° on average), while the largest difference is for the sp carbons α to the substituted sp^2 carbons (3.1° on average). The extent of the differences well represents the high bond-angle flexibility of sp-hybridized carbon atoms.[68] On the other hand, corresponding bond lengths are essentially the same between the planar and folded macrocyclic frameworks.

The pseudopolymorphism observed with **1a** clearly demonstrates that the dehydro[24]annulene framework can be "frozen" into various degrees of planarity in the crystalline state via non-covalent interactions. This conformational flexibility may be beneficial in a multi-fold topochemical polymerization reaction in that different manifolds of polymerization events can be expected depending on the macrocycle conformation and its solid-state arrangement, as proposed in our preliminary communication.[19] In addition, the experimental observations described above carry useful implications for subsequent crystal-engineering studies; i.e., the use of small, linear solvents such as MeOH or MeCN may promote the formation of the intended tubular assemblies, because these solvent molecules can effectively fill the inner cavity of the macrocyclic framework, thereby stabilizing the tubular structures. The size of CH_2Cl_2 appears to be at the upper limit of best fit, and the use of any larger or branched solvents will most likely result in non-tubular structures.

DOI: 10.1021/jacs.6b01939
J. Am. Chem. Soc. 2016, 138, 5939–5956

Crystal Packing of Benzoate Derivatives 1b−1f. Encouraged by the high solid-state stability and crystallinity of tetraol **1a**, we then synthesized the three hydroxybenzoate derivatives **1b−1d**, as well as the two iodobenzoate derivatives **1e** and **1f**, to study their crystal packing modes. Functionalized benzoate groups have been commonly employed as "handles" in molecules for the construction of topochemically polymerizable assemblies of linear oligoynes.[7]

Single crystals of 4-hydroxybenzoate **1b** were obtained as red plates by vapor diffusion of *n*-pentane into a THF solution. X-ray diffraction analysis revealed that **1b** crystallized with a unit-cell formula of **1b**·$(THF)_5$. The macrocyclic framework again has a planar conformation as expected from the red color of the crystals. All the substituents are nearly coplanar with the macrocyclic core, and the maximum deviation of a non-hydrogen atom in the substituents is only 0.85 Å from the mean plane of the macrocyclic framework. The four phenolic hydroxy groups are all hydrogen-bonded to THF oxygen atoms, with corresponding O···O distances of 2.62(1)−2.77(1) Å. As a consequence, there is no direct hydrogen bonding between hydroxy groups (Figure 4a). The one remaining THF molecule in the unit cell is engaged in an aryl−H···O(THF) contact with a H···O distance of 2.43(2) Å. Neighboring molecules of **1b** are interacting through cyclic double aryl−H···O=C interactions ($R_2^2(10)$ motif) and aryl−H···O−H contacts, where the corresponding H···O distances are 2.68(3) and 2.50(3) Å, respectively. Overall, these hydrogen-bonding interactions lead to the formation of a 2D extended sheet structure. The 2D sheets stack in such a way that the intersheet offset is approximately one macrocyclic-framework distance, with no channels seen in the resulting packing (Figure 4b). There are no direct short contacts between macrocyclic frameworks, and the only intersheet C···C short contacts are found between the alkynyl carbon C12 and the aryl carbon C16 with an interatomic distance of 3.275(3) Å (see SI). The inner cavity of each macrocyclic framework is occupied with a THF molecule from an adjacent layer either above or below with 50:50 probability. This uncertainty originates from the solvent disorder shown in Figure 4c,d. Given Nature's strong propensity to minimize void spaces in molecular crystals, it is reasonable to assume that this solvent arrangement, in which THF molecules effectively fill both the intermolecular spaces as well as the macrocyclic cavities, is an important factor in forming the observed interlayer registry.

Slow evaporation of a MeOH/acetone/H_2O solution of 3,5-dihydroxybenzoate **1d** resulted in the formation of red plates. Single-crystal X-ray diffraction analysis revealed that the molecular conformation of **1d** in the crystalline state is similar to that of 4-hydroxybenzoate **1b** (Figures 4a and 5a); Namely, the macrocyclic framework and the four substituents in **1d** are coplanar, and the maximum deviation of a substituent nonhydrogen atom from the mean plane of the macrocyclic framework is small, being only 0.37 Å. In contrast, the hydrogen-bonding motifs between these two crystal structures are very different. The hydroxy groups of **1b** are mainly involved in interactions with the occluded solvent molecules, whereas those of **1d** are mostly involved in direct interactions with neighboring macrocycles forming cyclic O−H···O=C interactions and O−H···O−H hydrogen bonds (O···O distances are 2.847(2) and 2.783(2) Å, respectively). Molecules are arranged to form a 2D extended sheet motif via these interactions (Figure 5a), which stack so that the two different types of vacant areas (inside and outside of the macrocyclic

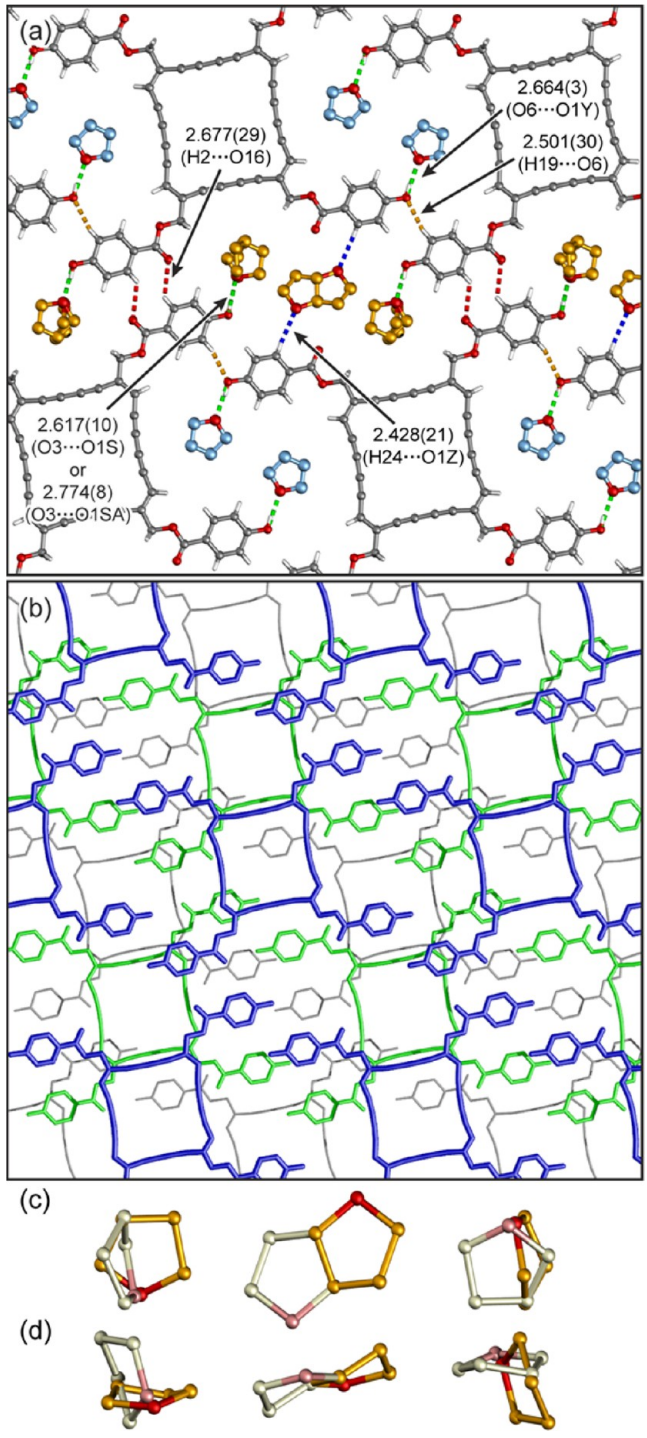

Figure 4. Representations of the crystal structure of **1b**. (a) Packing diagram showing the 2D extended sheet structure. Associated hydrogen bonds are indicated with dashed lines, and the corresponding interatomic distances are shown in angstroms. Hydrogen atoms of THF molecules are omitted for clarity. Molecules shown in yellow are disordered. (b) View perpendicular to the plane of macrocycles to show the registry between three consecutive sheet structures (top: navy, middle: green, bottom: gray). Hydrogen atoms and solvent molecules are omitted for clarity. (c,d) Disordered THF molecules viewed perpendicular to and along the plane of macrocycles, respectively. Two sets of molecular arrangements related by an inversion center are observed with a 50:50 probability, which are differentiated by dark and light colors. The two "standing" THF molecules in (d) fill the inner cavity of dehydroannulene framework in the next upper or lower sheet.

DOI: 10.1021/jacs.6b01939
J. Am. Chem. Soc. 2016, 138, 5939−5956

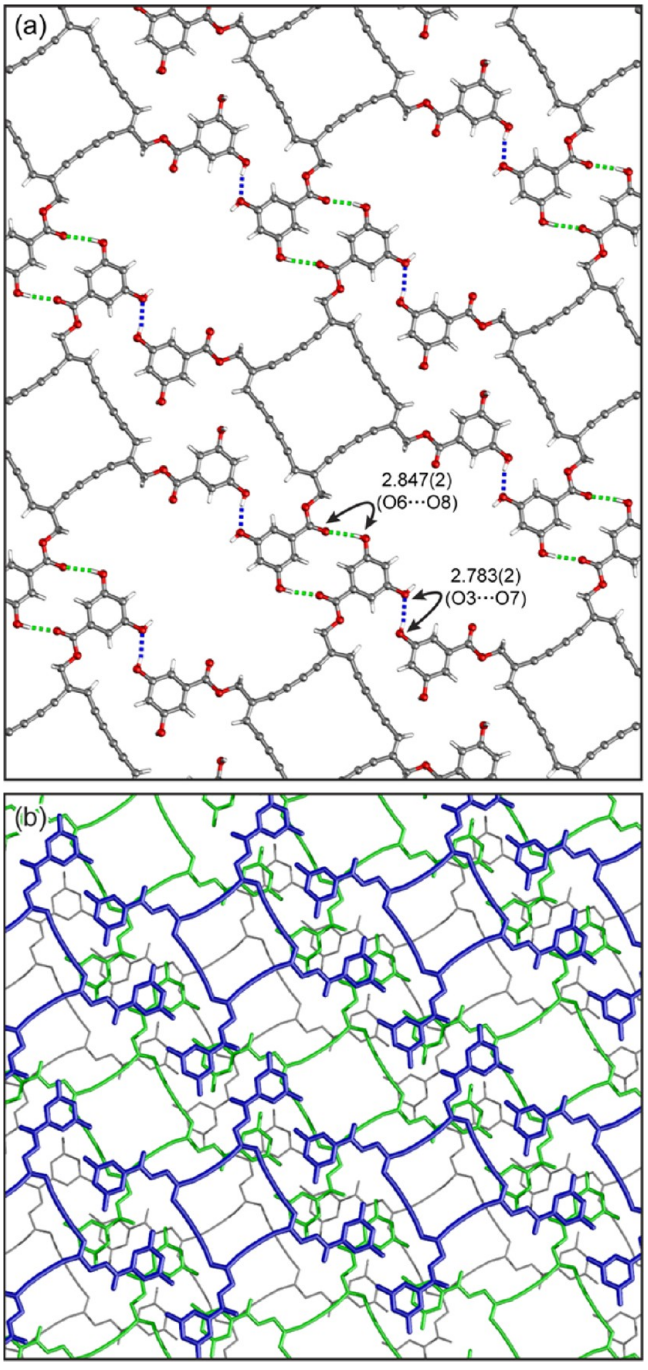

Figure 5. Representations of the crystal structure of **1d**. (a) Packing diagram showing the 2D extended sheet structure. Associated hydroxy hydrogen bonds are indicated with dashed lines. (b) View perpendicular to the plane of the macrocycle to show the registry between three consecutive sheet structures based on **1d** (top, navy; middle, green; bottom, gray). Hydrogen atoms and solvent molecules are omitted for clarity.

framework) are located approximately on top of each other (Figure 5b). The two types of voids are occupied with disordered solvent molecules. There are no direct short contacts between dehydro[24]annulene frameworks, and the shortest intersheet C···C contacts are found between carbonyl and aryl groups with an interatomic distance of 3.314(3) Å (see SI).

Single crystals of 3-hydroxybenzoate **1c** were obtained as red plates by vapor diffusion of *n*-hexane into a THF/CH_2Cl_2 solution. X-ray diffraction analysis showed that each 3-hydroxyphenyl group is disordered to adopt two different orientations in 1:1 ratio, and the group appears as if it was 3,5-dihydroxyphenyl on average. The packing of **1c** is very similar to that of **1d**, and hence it is not described in detail here; however, it is worth noting that the very different solvent systems used between the crystallizations of **1c** and **1d** provide essentially the same packing motif, pointing to the robustness of the associated intermolecular interactions.

Similarly to hydrogen bonding, halogen bonding is a highly directional non-covalent interaction[69] that is commonly used in the rational construction of supramolecular assemblies including those intended for topochemical polymerization.[7,70,71] In this study, we synthesized the two regioisomeric iodobenzoates **1e** and **1f** to examine their crystal-packing behavior. However, no single crystal of 4-iodobenzoate **1e** suitable for X-ray diffraction analysis was obtained despite multiple trials under different crystallization conditions. The very low solubility of **1e** led to the formation of powdery precipitates in all cases.

The 3-iodobenzoate **1f** is considerably more soluble than **1e**, and can be crystallized by slow diffusion of *n*-hexane into a CH_2Cl_2 solution to form red plates. Single-crystal X-ray diffraction analysis revealed that **1f** crystallized without incorporating any solvent molecules. The 3-iodophenyl moieties are slightly tilted against the planarized dehydro[24]-annulene framework by 29° or 34°, effectively filling the macrocyclic pores and inter-macrocyclic spaces in the crystal. Here, intermolecular I···C(sp) contacts with a distance of 3.619(2) Å are observed between I1 and C12 (Figure 6a). The aryl groups form isolated stacks, each of which is sandwiched between two dehydroannulene frameworks. The stack consists of four iodophenyl units from two neighboring molecules, and all the four aryl rings are parallel to each other having interplane angles of 0° or 5°. Their stacking distances are approximately 3.5 Å, as observed for common π-stacking assemblies such as hexabenzocoronenes.[72] Intermolecular iodine−iodine contacts are also observed (I1···I2 = 3.949(1) Å), each of which is accompanied by an Aryl−H···O═C interaction (H26···O2 = 2.57(3) Å) and an aryl−H···I contact (H26···I2 = 3.07(3) Å), as shown in Figure 6b. Two sets of these interactions connect neighboring molecules of **1f** to form a linear chain motif. The two I···I−C angles associated with the I···I contact are 90.9(1)° and 154.4(1)°. This arrangement slightly differs from the ideal right-angle mode for halogen−halogen bonding, in which the corresponding angles are 90° and 180°, respectively.[69] The deviation is assumed to be the result of compromise to gain the optimal total stabilization from the halogen- and hydrogen-bonding interactions associated with this intermolecular interaction motif.

The crystal structures of benzoate derivatives **1b**−**1d** and **1f** share a common feature—the planarized dehydro[24]annulene framework. This frequent appearance of the planar conformation, including the two pseudopolymorphs **1a-I** and **1a-II**, makes an interesting contrast to the previous observations in which nonplanar conformations are observed. For example, derivatives with small, non-hydrogen-bonding substituents such as acetoxymethyl[19] adopt nonplanar macrocyclic conformations in the crystalline state. The same is true for the parent dehydro[24]annulene[19] and its fully benzo-fused derivative.[73] Although it is still difficult to predict any solid-state

DOI: 10.1021/jacs.6b01939
J. Am. Chem. Soc. 2016, 138, 5939−5956

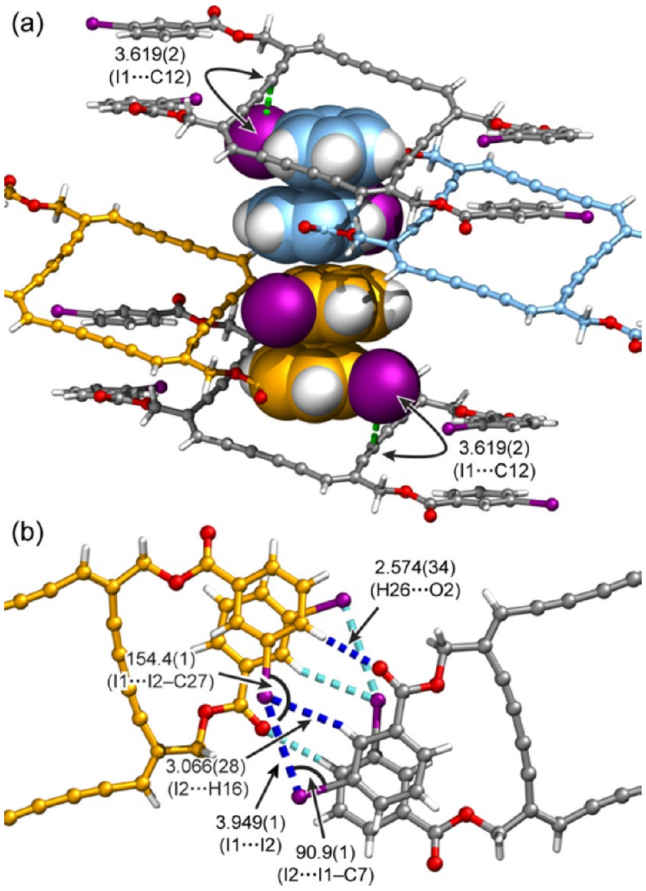

Figure 6. Representations of the crystal structure of **1f**. Selected interatomic distances and angles are shown in angstroms and degrees, respectively. (a) Packing diagram highlighting the quadruple aryl stack sandwiched between two dehydro[24]annulene frameworks. Associated I···C(sp) short contacts are indicated with green dashed lines. (b) Halogen- and hydrogen-bonding interactions observed between 3-iodophenyl moieties. The two complementary sets of three short contacts (I···I, I···H, and H···O) for each neighboring molecules lead to the formation of a 1D extended chain motif based on **1f**.

conformation of a macrocyclic framework, it is safe to say that a less stable, planarized conformation can be expected in future examples.

In contrast to the similarity of macrocyclic conformations in the examples above, the molecular-packing modes vary considerably between the benzoate derivatives depending on the substitution pattern of the aryl groups. Neighboring substituents in *meta*-hydroxybenzoates **1c** and **1d** form the self-complementary cyclic $R_2^2(14)$ motifs that involve both hydroxy and carbonyl groups thanks to the proper relative arrangement of these two functionalities. *meta*-Iodobenzoate **1f** also forms a self-complementary cyclic motif based on halogen and hydrogen bonding. In contrast, the hydroxy groups of *para*-hydroxybenzoate **1b** do not participate in any strong intermolecular interactions other than the hydrogen bonding with solvent molecules. Thus, where crystal engineering through a cocrystallization approach is concerned, it appears favorable that the "handles" on the compound of interest—hydroxy or iodo functionalities in the cases of benzoates **1b**–**1f**—are readily available for non-covalent interactions with other species. The formation of strong, self-complementary interactions between handle units (e.g., those observed for *meta*-functionalized derivatives **1c**, **1d**, and **1f**) is unfavorable in this context, perhaps because of the bent geometry of a *meta*-substituted benzene. Based on these considerations, we assumed that the *para*-substituted derivative **1b** would most easily influence the crystal packing mode through non-covalent interactions, whereas the other benzoate derivatives would not. This is discussed in the following section.

Crystal Engineering via a Host–Guest Strategy. *N,N′*-Disubstituted oxalamides are known to form 1D extended assemblies via hydrogen bonding. The repeat distance between hydrogen-bonded oxalamide units is ca. 5 Å, which matches the distance requirement for butadiyne topochemical polymerization shown in Scheme 1. Upon the installation of complementarily interacting functional groups between the oxalamide and dehydro[24]annulene components, it should be possible to form cocrystals in which the 5 Å repeat distance is transferred from the oxalamide assembly to the stack of dehydro[24]annulene molecules. Fowler, Laugher, Goroff, and their co-workers have successfully employed this host–guest strategy for the topochemical polymerization of various linear butadiyne derivatives, in which they achieved several remarkable single-crystal-to-single-crystal polymerizations revealed by X-ray diffraction.[7,28] In this study, we examined the cocrystallization of dehydro[24]annulenes **1a**–**1f** (guests) with *N,N′*-bis(pyridylmethyl)oxalamides **2a** and **2b** (hosts, Chart 2). Either hydroxy-to-pyridine (hydrogen-bonding) or iodine-to-pyridine (halogen-bonding) interactions were expected to operate in these host–guest combinations.

Chart 2. Structures of Oxalamide Derivatives 2a and 2b

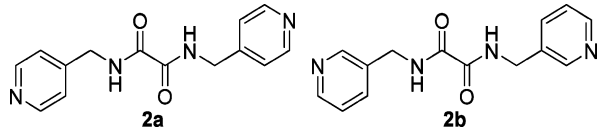

Cocrystals of 4-hydroxybenzoate **1b** and oxalamide **2b** were obtained as yellow needles from a THF/MeOH/MeCN mixed-solvent system. X-ray diffraction analysis revealed that the cocrystal has the monoclinic *C*2/*c* space group with $Z = 4$. As desired, oxalamide **2b** forms 1D stacks via hydrogen bonding with a repeat distance of 4.918(3) Å (Figure 7). This is successfully transferred to molecules of **1b** through phenol–pyridine interactions to afford a stacked, tubular array based on **1b** that extends along the crystallographic *b* axis. The cocrystal contains the two components in 1:1 ratio, even though the crystallization was set up with a molar ratio of **1b**:**2b** = 1:2. Only two of the four phenol groups in **1b** participate in phenol–pyridine interactions (O···N = 2.646(4) Å), while the other two form intermolecular phenol–phenol hydrogen bonds (O···O = 2.737(2) Å) (see SI). The macrocyclic framework is nonplanar in this case, and the inner cavity within each tubular structure is filled with solvent molecules highly disordered along the channel axis (axis *b*).

The two symmetry-nonrelated sets of butadiyne moieties are essentially equivalent in terms of the packing parameters relevant to the butadiyne topochemical polymerization—the observed values are the repeat distance $r = 4.9$ Å, tilt angle $\theta = 53°$, and C1···C4′ distance $d = 4.0$ Å (Figure 7b). Although the values of θ and d differ slightly from the optimal (45° and 3.5 Å, respectively), the obtained packing structure is within the range in which many butadiyne topochemical polymerizations can operate according to published examples. For example, 2,4-hexadiyne-1,6-diyl dibenzoate was reported to undergo

DOI: 10.1021/jacs.6b01939
J. Am. Chem. Soc. 2016, 138, 5939–5956

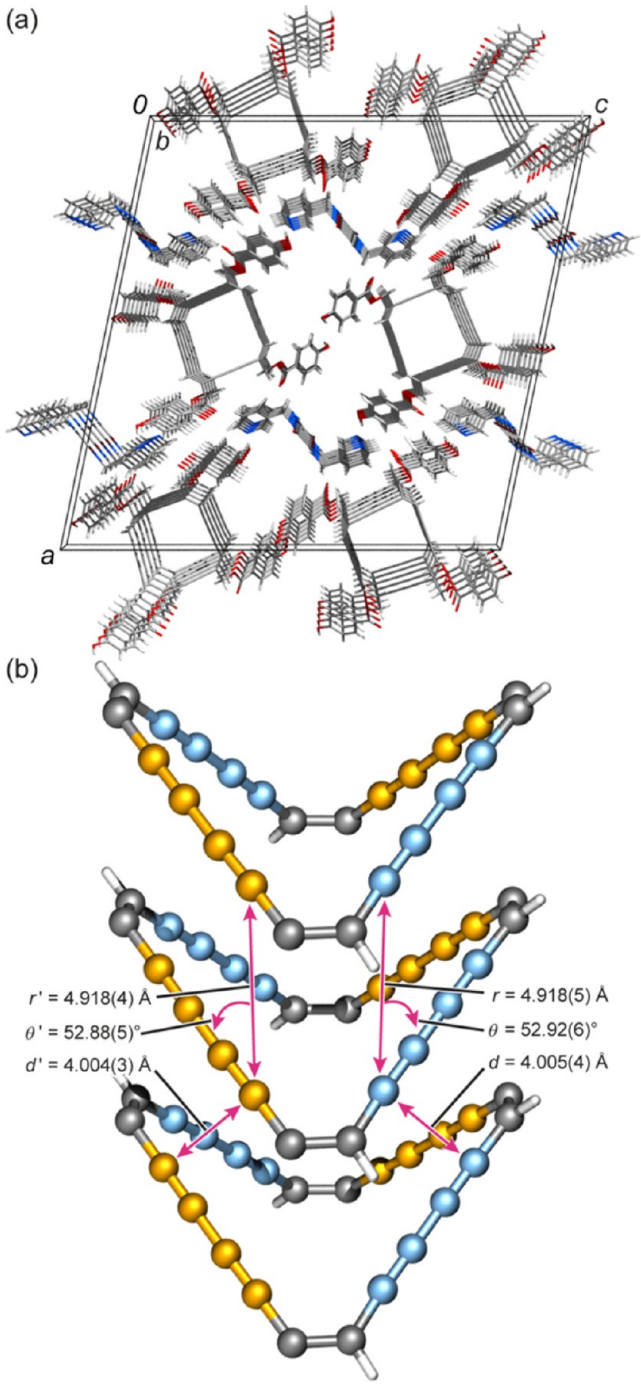

Figure 7. Molecular-packing diagrams for the cocrystal of **1b** and **2b**. (a) Perspective view along the column axis, or the crystallographic *b* axis. (b) Close-up view of three consecutive dehydro[24]annulene frameworks within a tubular stack. Nonequivalent butadiyne units are differentiated by light blue and yellow. Packing parameters relevant to butadiyne topochemical polymerization are shown in angstroms or degrees. Substituents are omitted for clarity.

pressure-induced topochemical polymerization in the crystalline state. Its monomeric units are aligned with packing parameters of r = 4.3 Å, θ = 59°, and d = 4.0 Å.[74] Another study involved two different diiodobutadiyne–oxalamide (**2a** or **2b**) cocrystals with packing parameters of r = 5.1 Å, θ = 51°, d = 3.9 Å, or r = 5.0 Å, θ = 65°, d = 4.9 Å.[75] Both cocrystals were also found to undergo topochemical polymerization under high-pressure conditions. Additionally, it has been suggested that the repeat distance r is more important than the C1···C4′ distance d in determining the success of topochemical polymerizations.[75,76] Thus, the tubular packing obtained in the present case (r = 4.9 Å) is highly promising for our intended polymerization.

Contrary to 4-hydroxybenzoate **1b**, the other benzoate derivatives **1c**–**1f** did not form cocrystals suitable for single-crystal X-ray analysis with either oxalamide **2a** or **2b**. All our attempts resulted in the formation of crystals of either of the two separate components, or the precipitation of powdery solids. As described earlier, **1b** is the only derivative whose "handles" are left available for solvents, in that they are not participating in any strong, self-complementary interactions. Thus, it is presumed that the reluctance of **1b** to form strong self-associative interactions facilitates the formation of cocrystals with host molecules. A related observation has been reported by Fowler, Lauher and co-workers, in which the thermodynamic stability associated with self-hydrogen-bonded packing of 4,4′-(oxalyldiimino)dibutyric acid was suspected as the reason why this compound did not cocrystallize with dipyridyldiacetylenes.[56] Although the experimental observations by others and us do not yet provide a general rule, these results point out the importance of carefully examining crystal structures of each component in designing host–guest cocrystals.

Another cocrystallization was achieved in the combination of tetraol **1a** and oxalamide **2a**. The crystals were grown by vapor diffusion of *n*-pentane into a THF/MeOH solution containing **1a** and **2a** in 1:2 molar ratio. Single-crystal X-ray diffraction analysis revealed that the crystal has the triclinic P space group with Z = 1 and the formula **1a**·**2a**. There are no solvent molecules occluded in the cocrystal, and the pyridyl groups of **2a** effectively fill the cavities of planarized macrocyclic frameworks of **1a**. These pyridyl groups form energetically favorable antiparallel, rather than parallel, π dimers[77] with an associated plane-to-plane distance of 3.45 Å. Unexpectedly, the molecules of oxalamide **2a** form neither the commonly observed oxalamide–oxalamide interaction nor any direct hydrogen bonds to each other. Instead, each molecule of **2a** is engaged in six hydrogen-bonding interactions with neighboring molecules of **1a**; namely, two N–H···O–H (N2···O1 = 2.978(2) Å), two C═O···H–O (O2···O3 = 2.754(1) Å), and two N(pyridyl)···H–O interactions (N1···O1 = 2.849(2) Å) (Figure 8a, green dashed lines). The sextuple hydrogen-bonding motif ties up the planarized macrocycles to form a 2D extended sheet structure. Adjacent molecules of **1a** have short C(sp^2)···C(sp^2) contacts of 3.382(2) Å (Figure 8a, red dashed lines). The planarized dehydro[24]annulene framework is considerably distorted from the near-square configurations observed in **1a-I** and **1a-II** (Figures 1a and 2a, respectively) into a rhombus shape (Figure 8b). The two nonequivalent substituted sp^2 carbons in **1a**·**2a** have considerably different bond angles (121.6(1)° for C5 and 125.5(1)° for C10), and sp carbons C9 and C9′ are bent from linearity by more than 15°. This significant in-plane distortion of the macrocyclic framework is probably there to accommodate the multiple hydrogen-bonding interactions between **1a** and **2a**. They are most likely enabled by the high flexibility of acetylene units in the dehydro[24]annulene framework.[68]

The cocrystals of **1a**·**2a** do not form the expected host–guest assembly. In a host–guest strategy, the host is expected to dictate the packing of the guest, and thus a distinct hierarchy can be ascribed between the two components. In cocrystals of

DOI: 10.1021/jacs.6b01939
J. Am. Chem. Soc. 2016, 138, 5939–5956

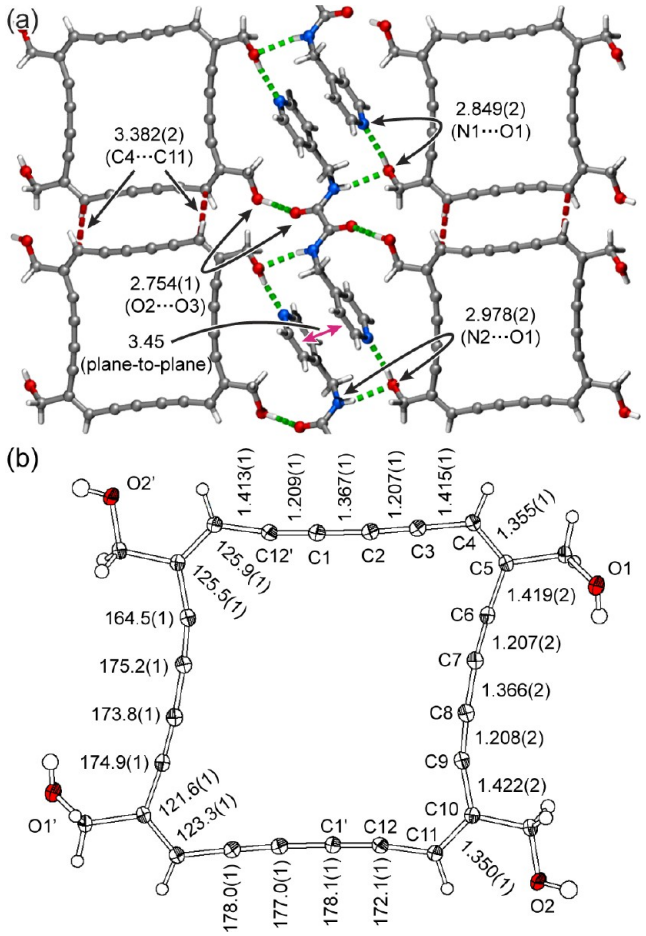

Figure 8. Representations of cocrystal **1a·2a**. Selected interatomic distances and bond angles are shown in angstroms and degrees, respectively. (a) Molecular packing viewed approximately perpendicular to the 2D extended sheet structure. Hydrogen bonds are shown with green dashed lines, and short C···C contacts with red dashed lines. (b) Thermal ellipsoid plot of **1a** in the cocrystal at 50% probability.

1a·2a, the two components mutually affect each other and essentially *collaborate* to form a unique packing motif for this specific combination. An obvious and important factor that facilitates the formation of what we can term "collaborative cocrystals" is the structural matching between the involved components so as to accommodate stabilizing complementary interactions. In relation to this, it is worth reporting that our attempts to grow cocrystals of tetraol **1a** with oxalamide **2b**, a regioisomer of **2a**, resulted in the formation of discrete crystals of either of the two compounds. Another factor that potentially operates in the formation of cocrystals of **1a·2a** is the insufficient differentiation in the strengths of hydrogen bonds between the donor and acceptor. Specifically, the hydrogen-bond-donating abilities of the hydroxymethyl moieties of **1a** and the amide groups of **2a** may be similar enough to perturb the formation of the desired oxalamide−oxalamide interaction under the given crystallization conditions. This assumption is consistent with the earlier example of host−guest assembly **1b·2b**, in which all the stronger hydrogen-bond donors (phenolic hydroxy groups) selectively interact with the stronger hydrogen-bond acceptors (pyridyl nitrogen atoms). Thus, even though the combination of the hydroxy−pyridine and the oxalamide−oxalamide interactions is known to be an effective setup for the formation of host−guest assemblies,[78] fine-tuning of the hydrogen-bond donor/acceptor strengths[79] may still be needed to resolve difficult cases such as the present one.

Crystal-Packing Behavior of Carbamate Derivatives 1g−1j. Another strategy to achieve favorable molecular packing for a diacetylene topochemical polymerization is to covalently introduce functional groups that provide the appropriate repeat distances of around 4.9 Å in crystals. Based on this approach, a number of linear butadiyne derivatives have been successfully organized to form topochemically polymerizable assemblies in single crystals,[30,80−84] liquid crystals,[85] or organogels.[27,29,31,32,86−88] Although macrocyclic systems are significantly underrepresented compared to linear ones, there are several successful examples currently known.[25,35,37,38,40,41]

In the present study, we synthesized tetracarbamate derivatives **1g−1j** and examined their packing behavior in the crystalline state. The carbamate−carbamate hydrogen-bonding motif is among the most commonly used interactions in diacetylene topochemical polymerization.[80,81,83,84,88,89] Additionally, previous experimental observations suggest that it is preferable to have an odd number of methylene units between a rigid reacting core and a carbamate moiety in order to obtain an adequate tilt angle (ca. 45°) between the butadiyne units.[80] Thankfully, and in accordance with this observation, each carbamate group in derivatives **1g−1j** is linked through a single methylene unit to the macrocyclic core.

Slow evaporation of a THF/MeCN solution of benzyl carbamate **1g** resulted in the formation of light-yellow needles. Single-crystal X-ray diffraction analysis revealed that **1g** crystallizes in the chiral space group *C*2 with $Z = 2$ under these conditions. In fact, two pseudopolymorphs of **1g** were obtained, and this is the first structure that is referred to as **1g-I**.

As desired, the macrocycles form beautiful columnar stacks via a four-fold hydrogen-bonding network (Figure 9). The narrow cavities both inside and outside of the dehydro[24]-annulene-based tubular stacks are filled with severely disordered solvent molecules, most likely MeCN. As expected from the light-yellow color of the crystals, the macrocyclic framework adopts a folded conformation in this case. The butadiyne units of **1g** are arranged in a similar manner to that observed in the cocrystal of **1b·2b**. In the case of **1g-I**, the observed packing parameters for the two symmetry-nonrelated sets of butadiyne units are repeat distance $r = 4.8$ Å, tilt angle $\theta = 53°$, C1···C4′ distance $d = 4.1$ Å, or $r = 4.8$ Å, $\theta = 55°$, $d = 4.0$ Å (Figure 9b). On the other hand, the arrangement of substituents in the crystal structures of **1g-I** and **1b·2b** is considerably different. The allyloxy moieties (−C═C−CH_2−O−) are almost coplanar in the cocrystal **1b·2b** (the C−C−C−O dihedral angles are 2.5(3)° and 2.8(3)°), whereas they adopt near right-angle dihedrals in the columnar stacks of **1g** (115.9(5)° and 115.6(5)°). These observations indicate that the hydroxymethyl substituent conformation does not have a significant effect on the macrocyclic arrangement within columnar stacks.

A completely different packing motif resulted when benzylcarbamate **1g** was crystallized by slow diffusion of cyclohexane into a THF solution. Single crystals of pseudopolymorph **1g-II** are yellow blocks, and X-ray diffraction analysis revealed that the crystal has the orthorhombic $Pca2_1$ space group with $Z = 4$. In this case, the carbamate hydrogen bonds of pseudopolymorph **1g-II** led to the formation of a 2D extended sheet structure (Figure 10) in contrast to the 1D extended columnar motif observed for **1g-I**. The difference in

DOI: 10.1021/jacs.6b01939
J. Am. Chem. Soc. 2016, 138, 5939−5956

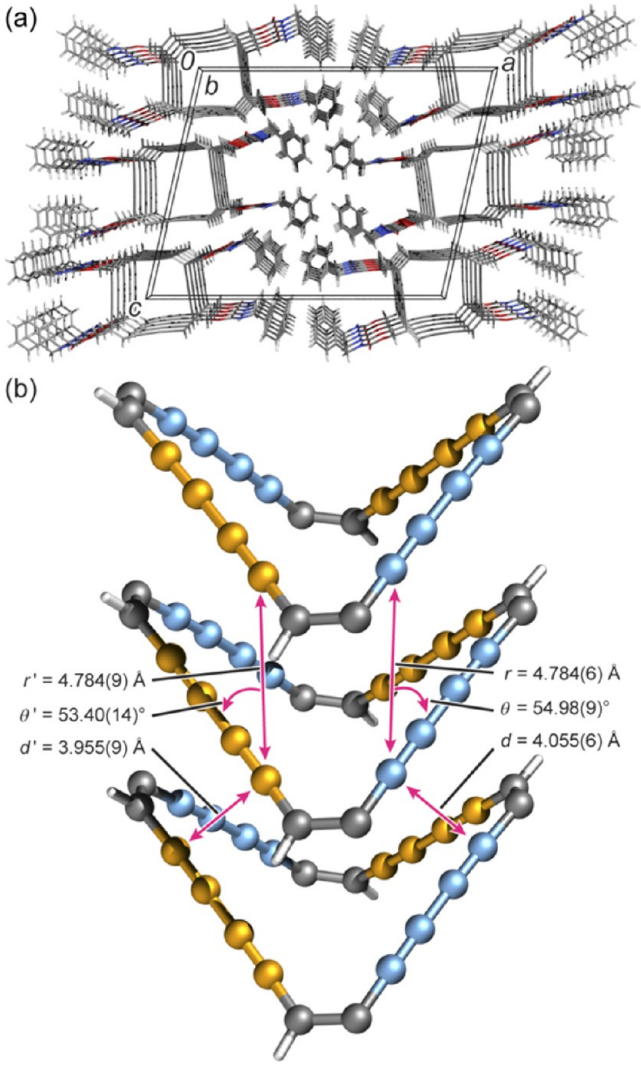

Figure 9. Representations of pseudopolymorph **1g-I**. (a) Perspective view along the crystallographic *b* axis. Each dehydro[24]annulene-based tubular structure is associated with four linear hydrogen-bonding networks of carbamate units along the *b* axis. Substituents are partially disordered and only the main conformations are shown. (b) Close-up view of three consecutive dehydro[24]annulene frameworks within the tubular motif. Non-equivalent butadiyne units are differentiated by light blue and yellow. Packing parameters relevant to butadiyne topochemical polymerization are shown in angstroms or degrees. Substituents are omitted for clarity.

crystal-packing modes appears to be largely related to the availability of a small, linear solvent such as MeCN, which can stabilize tubular structures by filling their inner cavity, as discussed earlier. The dehydro[24]annulene-based sheet structure is formed via carbamate−carbamate hydrogen-bonding networks extending along the crystallographic *a* axis (Figure 10a,b). Each of the dehydroannulene-based sheet structures is "sandwiched" between benzyl-group layers (Figure 10a). The spaces between the macrocyclic framework and the benzyl groups are filled with cyclic solvent molecules (most likely cyclohexane and/or THF), some of which could not be refined properly because of severe disorder.

There are many short C···C contacts between dehydro[24]-annulene frameworks in pseudopolymorph **1g-II**. Ten of the 24 carbons in each framework are in contact with neighboring frameworks, with the shortest interatomic distance of 3.222(3) Å for C4···C16 (Figure 10c). In spite of these many short contacts, the crystals of **1g-II** were stable in the mother liquor at 25 °C for at least a month, and they did not show any explosive behavior upon mechanical stimuli. This is in stark contrast to the extremely high reactivity of the parent dehydro[24]annulene in the solid state, which explodes upon touching with a needle or laboratory spatula.[19] Six of the macrocyclic carbons in the parent dehydro[24]annulene are similarly engaged in intermolecular short C···C contacts in the single-crystalline state. The high stability of **1g-II** is probably due to the tight molecular packing mediated by the multiple hydrogen-bonding networks, which may provide considerable resistance against crystal-packing deformation associated with potential solid-state reactions. It is also worth pointing out that near-parallel sequences of butadiyne units are observed along axis *a*, in which neighboring units are not translationally equivalent, but related by a glide plane (Figure 10c,d). The associated repeat distance is 5.255(3) Å (calculated as the inter-centroid distance, shown as *r* in Figure 10d), and the C1···C4′ distance is 3.358(3) Å. It has been reported that glide-plane-related butadiyne units of deca-4,6-diyne-2,9-diyl bis-(phenylcarbamate) undergo topochemical polymerization.[81] However, the polymerization seems unlikely in **1g-II** because the reaction would cause unfavorable deformation of molecular structure and crystal packing as mentioned above. Indeed, **1g-II** did not show any sign of topochemical polymerization upon heating up to 120 °C or by UV irradiation at 254 nm.

The pseudopolymorphism of benzyl carbamate **1g** implies that the two hydrogen-bond mediated packing motifs (i.e., the column and sheet motifs) based on the tetracarbamate system are close in energy. Thus, it should be possible to alter crystal-packing patterns between these two motifs not only by changing crystallization solvents, but also by changing substituent structures. This assumption was experimentally confirmed—when the *N*-substituents were changed from benzyl to *n*-hexyl, a sheet motif was selectively formed even in the presence of a small, linear solvent. Specifically, slow diffusion of MeCN into a THF solution of *n*-hexylcarbamate **1h** provided yellow plates, which possess the molecular packing shown in Figure 11. Similarly to the case of **1g-II**, the carbamate hydrogen bonds of **1h** form a 2D extended sheet motif along the *ab* plane. Here again, the crystals of **1h** are stable at room temperature despite numerous short C···C contacts between macrocyclic frameworks. In this case, 12 of the 24 carbon atoms in each macrocyclic framework are in close-contact with neighboring frameworks, with the shortest contact of 3.253(5) Å (see SI). The *n*-hexyl groups are interdigitated to effectively fill the space between dehydro[24]-annulene-based sheet structures, and there are no solvent molecules incorporated in the crystal. Because of this interdigitation, the sheet structures form a slipped stack that fits in the triclinic *P* space group, while the layers in **1g-II** stack straight to fit in the orthorhombic space group.

Phenylcarbamate **1i**, on the other hand, forms again the expected columnar motif (Figure 12). Slow diffusion of MeOH into a THF solution of **1i** resulted in the precipitation of light yellow needles. Single-crystal X-ray analysis revealed that **1i** crystallized in the tetragonal *I* space group, and the macrocyclic framework is slightly flattened in comparison to the other folded conformations described above. The stacking pattern of **1i** is unlike the two previously described columnar structures of **1b** (Figure 7) and **1g** (Figure 9) in that molecules of **1i** stack alternatively within a column. Thus, each column based on **1i** is

DOI: 10.1021/jacs.6b01939
J. Am. Chem. Soc. 2016, 138, 5939−5956

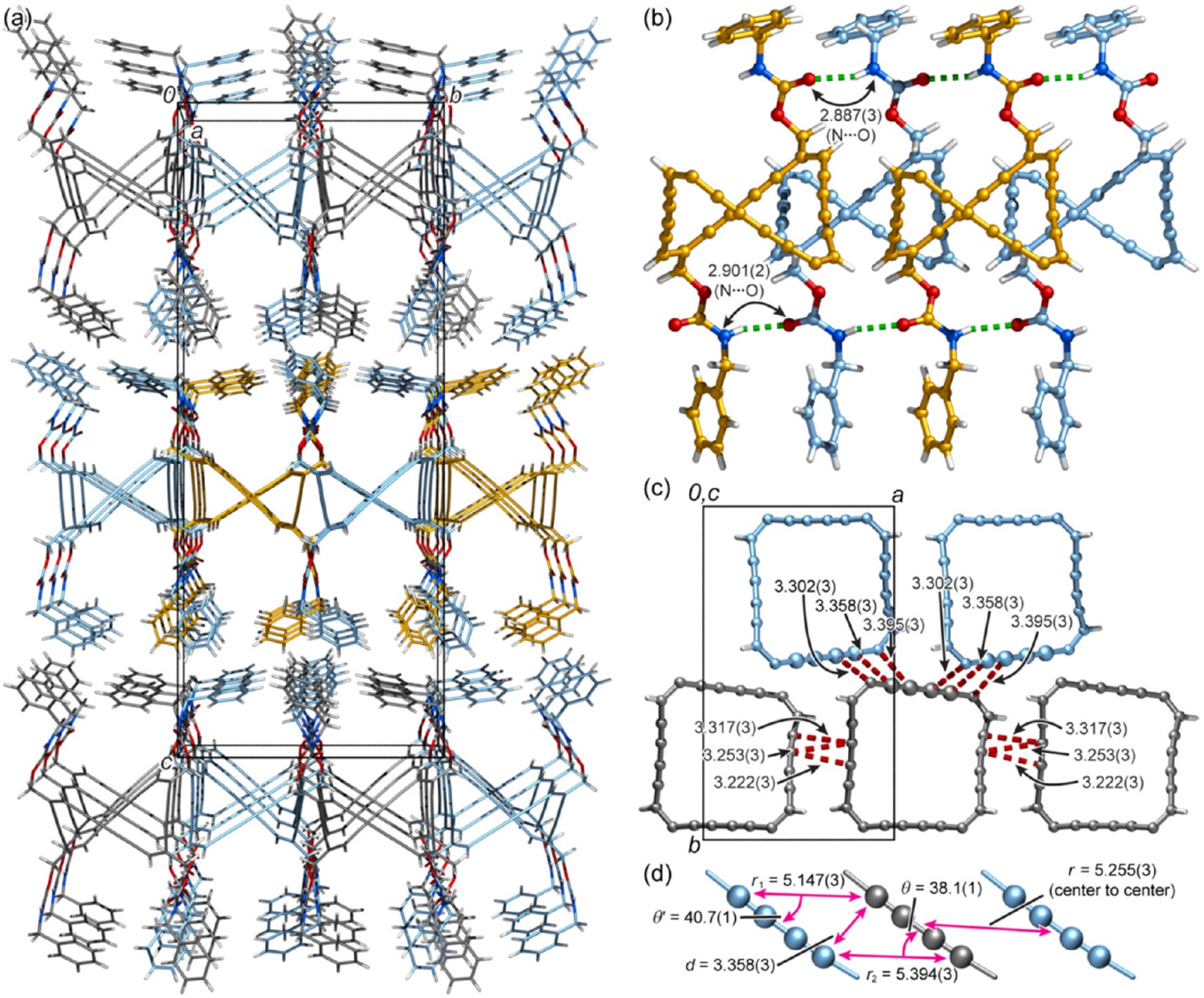

Figure 10. Molecular-packing representations of pseudopolymorph **1g-II**. The colors of carbon atoms are differentiated based on the symmetry operations that correlate molecules: gray, identity; yellow, two-fold screw axis; light blue, glide plane. Salient distances and angles are shown in angstroms and degrees, respectively. Substituents are partially disordered and only the main conformation is shown. (a) Perspective view along the crystallographic *a* axis. The 2D-sheet motif extends along the *ab* plane. (b) Packing diagram perpendicular to the *a* axis, highlighting the hydrogen-bonding networks of carbamates (green dashed lines). Only two substituents per molecule are shown for clarity. (c) Arrangement of dehydro[24]annulene frameworks within the sheet structure viewed along the *c* axis. Short C···C contacts associated with one macrocyclic framework (bottom-middle) are indicated by red dotted lines. Substituents are omitted for clarity. Atoms highlighted with larger balls corresponds to the carbon atoms shown in (d). (d) Close-up view of the butadiyne-unit sequence extending along axis *a*. Neighboring units are related by a glide plane.

racemic and associated with a four-fold rotoinversion axis at its center along the crystallographic *c* axis (Figure 12a). The carbamate−carbamate hydrogen bonds in this structure form zigzag chains, rather than the straight chains observed in pseudopolymorph **1g-I**. Accordingly, the repeat distance between the stacked butadiyne units of **1i** is only 4.2 or 4.3 Å (center-to-center distances between neighboring butadiyne units, Figure 12b), being considerably shorter than the corresponding distances in the two former cases of **1b** and **1g** (4.9 and 4.8 Å, respectively). Furthermore, the associated tilt angles (62−63°) and the C1···C4′ distances (ca. 4.2 Å) are considerably larger than the optimal values for butadiyne topochemical polymerization (45° and 3.5 Å, respectively, Scheme 1). Although the reasons for this alternating/non-alternating variation between **1g** and **1i** are unclear,[83,90,91] it is evident that the conformational flexibility of the dehydro[24]-annulene framework is an important factor in providing the large diversity of packing motifs seen in this work.

An extreme case of macrocyclic conformation was observed for *p*-methoxyphenyl carbamate **1j** (Figure 13). Single crystals of **1j** were obtained as red prisms by slow diffusion of acetone into a THF solution. X-ray diffraction analysis revealed that **1j** crystallized into the triclinic *P* space group with **1j**·(acetone)$_4$ stoichiometry. As expected from the red color, the macrocyclic framework adopts a planar conformation. Two of the four substituents on each macrocycle are coplanar with the macrocyclic framework, while the other two are near perpendicular to the framework and antiparallel to each other (Figure 13b). Overall, the molecule has a windmill-like conformation associated with an inversion center in the middle

DOI: 10.1021/jacs.6b01939
J. Am. Chem. Soc. 2016, 138, 5939−5956

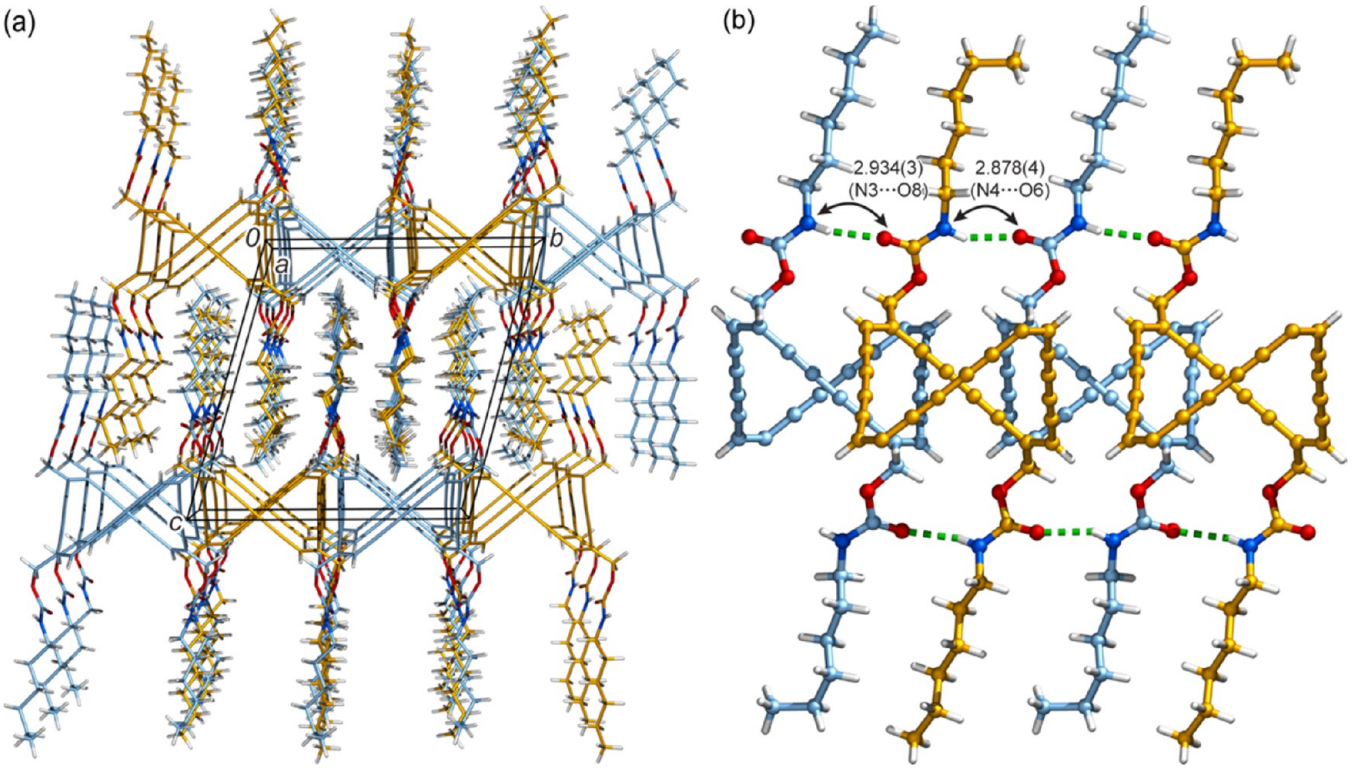

Figure 11. Representations of the crystal structure of **1h**. The molecules differentiated by light blue and yellow correlate with each other by inversion. One of the four *n*-hexyl groups per molecule is disordered to adopt two different conformations, and only the main conformation is shown. (a) Perspective representation along the *a* axis. The hydrogen-bond-mediated 2D-sheet motif extends along the crystallographic *ab* plane. (b) Packing diagram perpendicular to the *a* axis, highlighting two hydrogen-bond networks of carbamate units (green dashed lines). The corresponding hydrogen-bond distances are shown in angstroms. Substituents are partially omitted for clarity.

of the macrocyclic framework. Unexpectedly, there is no direct hydrogen bonding between the carbamate groups of **1j**, and instead each carbamate hydrogen atom interacts with a carbonyl oxygen of the occluded acetone (N···O = 2.982(1) or 2.910(2) Å, green dashed lines in Figure 13a). The acetone molecules also serve as hydrogen-bond donors toward the carbamate carbonyls (C···H = 2.40(2) or 2.59(3) Å, only the former is shown in Figure 13a with blue dashed lines). Neighboring molecules of **1j** interact through self-complementary O···H contacts involving two C(vinyl)−H···O(ether) interactions (H7···O6 = 2.51(2) Å) and two C(aryl)−H···O═C interactions (H26···O5 = 2.42(2) Å) as shown in Figure 13a with red dashed lines. The sequence of this hydrogen-bonding motif leads to a zigzag-chain structure extending along the crystallographic *c* axis. In addition, there are a number of other hydrogen bonds and C−H···π interactions between the zigzag-chain structures (see SI).

The crystal structures of **1g**−**1j** explicitly demonstrate that the *N*-substituent of carbamate moieties has strong impact over the crystal-packing behavior of these dehydro[24]annulene tetracarbamate systems. The rich diversity in crystal-packing modes and the significant variation in the associated hydrogen-bond motifs are remarkable, given that all these compounds share the same core structure (the dehydro[24]annulene framework) and the same type of hydrogen-bonding functionality (the carbamate group). In fact, a case in which no direct hydrogen bonding between carbamate groups is even observed (derivative **1j**). This crystal-packing diversity is likely the result of the rotational freedom of the methylene hinges in addition to the flexibility of the dehydro[24]annulene framework. Indeed, the allyloxy moieties adopt a wide range of dihedral angles in order to accommodate favorable hydrogen-bonding interactions. For example, the substituents in **1g-I** are oriented "exo" to the nonplanar macrocyclic framework with allyloxy torsion (C−C−C−O) angles of −115.9(5)° and −115.6(5)°, while those in **1g-II** are directed "endo" with the corresponding torsion angles of ±127.6(2)°. In the case of **1j**, the observed allyloxy torsion angles are ±1.1(2)° and ±132.9(1)°

Transfer integral analysis. Columnar π-stacks allow efficient exciton and charge-carrier migration along the column axis. For example, Zang, Moore, and co-workers reported that nanofibril self-assemblies of arylene ethynylene macrocycles could be used for explosive sensing based on a fluorescence quenching mechanism.[92] The high sensitivity of the system was assumed to originate from the efficient exciton migration in columnar stacks. In addition, the authors pointed out the importance of the intrinsic porosity originating from the macrocyclic molecular structure in terms of analyte diffusion within the film. Charge-carrier mobility in 1D columnar π-stacks was also explored in many theoretical and experimental studies.[9,93−103] The high sensitivity of charge-carrier mobility to local molecular arrangement was highlighted in, among others, the 2009 report by Müllen, Andrienko, and co-workers.[94]

For the purpose of examining the extent of intermolecular electronic coupling, we calculated the transfer integrals of the columnar motifs obtained in this work. Although calculated transfer integrals cannot always be linked directly to experimental charge-carrier mobilities, they serve as useful indicators of the strength of intrinsic electronic coupling

DOI: 10.1021/jacs.6b01939
J. Am. Chem. Soc. 2016, 138, 5939−5956

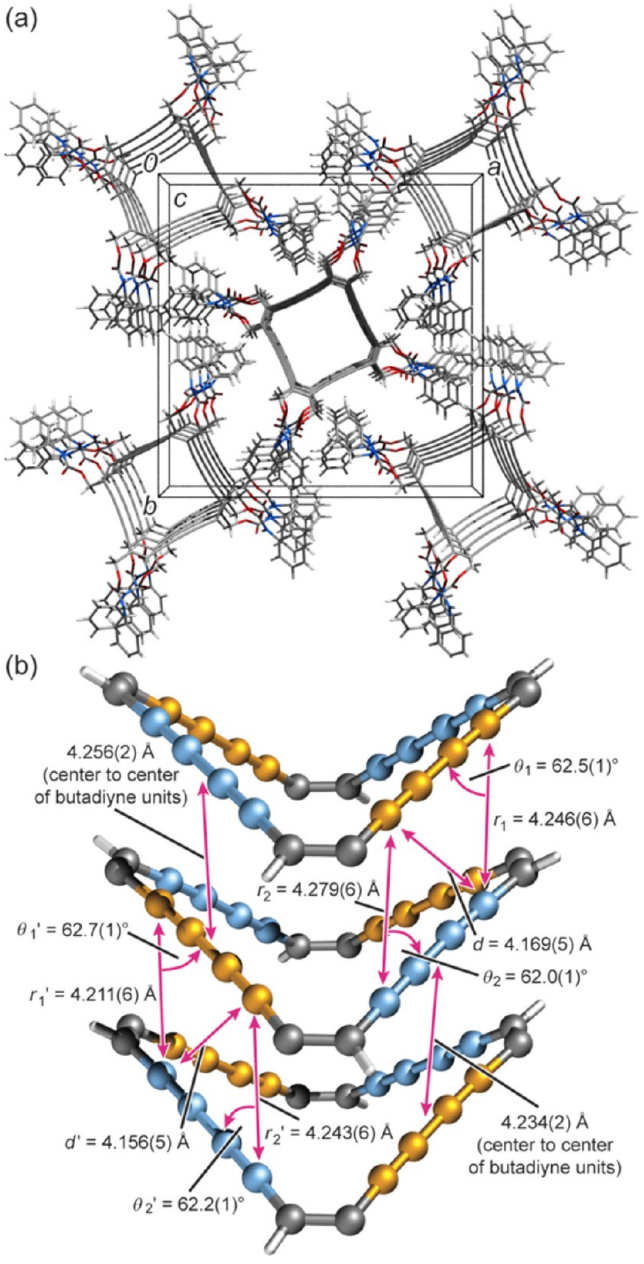

Figure 12. Representations of the crystal structure of phenylcarbamate **1i**. (a) Perspective view along the *c* axis. Each dehydro[24]annulene-based columnar structure is associated with four threads of carbamate hydrogen-bonding networks formed along the *c* axis. A four-fold rotoinversion axis runs through the center of each column along the *c* axis, and neighboring columns are related by a two-fold screw axis. Substituents are partially disordered and only the main conformations are shown. (b) Three consecutive dehydro[24]annulene frameworks within a columnar stack. Non-equivalent butadiyne units are differentiated by light blue and yellow. Packing parameters relevant to butadiyne topochemical polymerization are shown in angstroms or degrees. Substituents are omitted for clarity. Note that the positions of the hydrogen atoms switch between neighboring frameworks because of the alternating-stack mode.

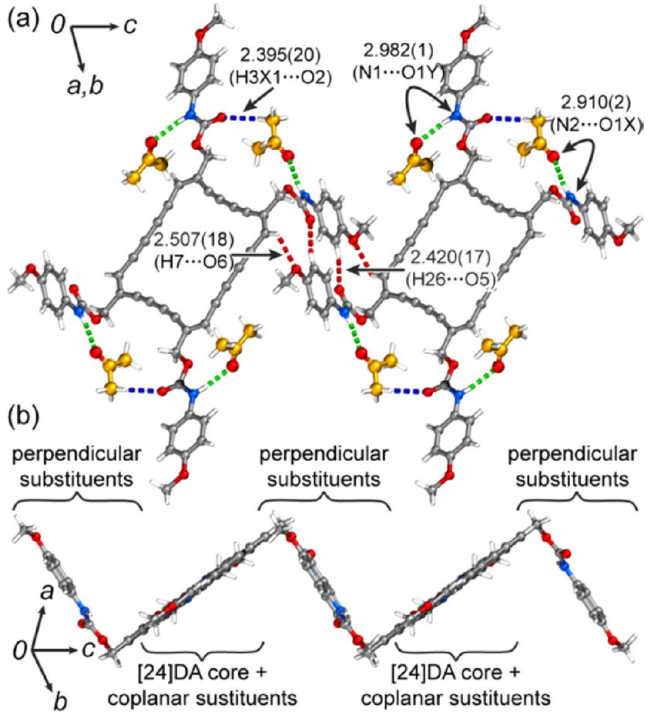

Figure 13. Representations of the crystal structure of **1j**. (a) View parallel to the *ab* plane. Selected distances are shown in angstroms. The self-complementary quadruple hydrogen-bond interactions between molecules of **1j** are highlighted with red dashed lines. The occluded acetone molecules serve as both hydrogen-bond acceptors (green dashed lines) and donors (blue dashed lines). (b) Side view of the same portion of the zigzag chain motif as shown in (a).

between neighboring molecules. Here, we employed the PW91 functional with a Slater-type triple-ζ plus polarization (TPZ) basis set, which has been shown to give reliable results.[104,105]

Figure 14 shows the calculated transfer integrals for the highest occupied molecular orbitals (HOMOs) and the lowest unoccupied molecular orbitals (LUMOs). The highest values are observed in the case of compound **1g**; transfer integrals for HOMOs (t_H) and LUMOs (t_L) are 98.3 and 96.8 meV, respectively (Figure 13b). This t_H value exceeds those calculated for high-performance p-type semiconductors such as pentacene (79.3 meV) or rubrene (90.5 meV) (Figure S52a,b). In addition, the t_L value is comparable to that of 6,13-bis(triisopropylsilylethynyl)-5,7,12,14-tetraazapentacene (102.5 meV), a high-performance n-type semiconductor (Figure S52c). The other columnar structures obtained in this work gave considerably different values (Figure 14a,c), reflecting that minor variations in the relative arrangement of neighboring molecules can greatly affect those values.[17,94,106] Importantly, a shorter repeat distance between the macrocycles does not necessarily lead to a larger transfer integral, as can be seen in the cases of **1g** (r = 4.78 Å) and **1i** (r = 4.23 Å). It is known that intermolecular electronic interactions can be optimized through the control of relative offsets or rotation angles between neighbors for planar π-systems.[17,94,106] For nonplanar π-systems, as in the case of the dehydro[24]annulenes, one also needs to carefully optimize the degree of framework folding to achieve favorable orbital−orbital interactions.

CONCLUSION

Three different tubular architectures based on the dehydro[24]-annulene framework were obtained as part of the present crystal-engineering study. These supramolecular structures are among the rare examples of isolated (i.e., non-intermeshed) dehydroannulene-based columnar stacks.[45,52,107,108] They are also the first examples of columnar supramolecular architec-

DOI: 10.1021/jacs.6b01939
J. Am. Chem. Soc. 2016, 138, 5939−5956

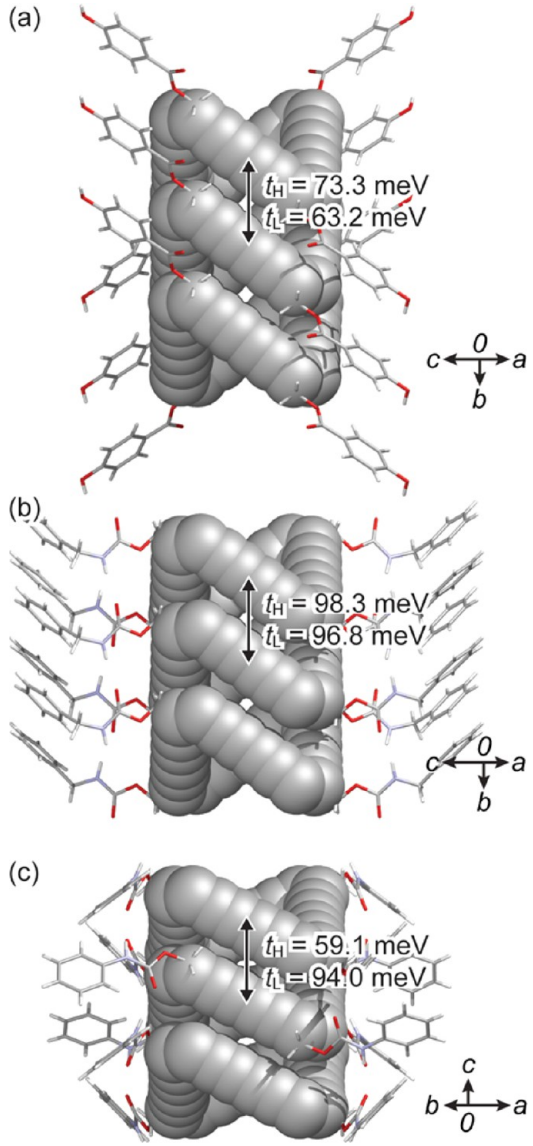

Figure 14. Transfer integrals between HOMOs (t_H) or LUMOs (t_L) calculated at the PW91/TZP level of theory for the columnar assemblies based on **1b** (a), **1g** (b), or **1i** (c).

tures based on flexible, nonplanar dehydroannulenes with solvent-accessible inner space. Gratifyingly, the tubular assemblies obtained with derivatives **1b** or **1g** possess close-to-ideal packing parameters for the intended multi-fold topochemical polymerization. Thus, the nanotubular materials proposed in Scheme 1 may be within reach. Furthermore, the calculation of transfer integrals indicates that dehydroannulenes with nonplanar conformations may have significant electronic coupling in the solid state upon careful optimization of the molecular arrangement, and thus, should be suitable for detection studies on gaseous or explosive molecules.

In addition to the nanotubular assemblies, a wide variety of dehydro[24]annulene-based molecular architectures were obtained, such as an array of nanochannels (**1a-I**), stacked sheets with solvent-filled pores (**1b**–**1d**), and lamellar assemblies (**1g-II** and **1h**). The significant diversity in packing modes arises from the conformational flexibility of the macrocyclic core and the rotational freedom of the methylene hinges. Indeed, the flexibility of the dehydro[24]annulene core is clearly demonstrated with the pseudopolymorphs of tetraol **1a**, in which the macrocyclic framework adopts either planar (**1a-I** and **1a-II**) or nonplanar (**1a-III**) conformations. In addition, the planarized macrocyclic framework in the cocrystal **1a**•**2a** shows considerable in-plane deformation from a square to a rhombus shape that is solely induced through non-covalent interactions. The pseudopolymorphs of **1a** are associated with different motifs of intermolecular hydroxy hydrogen bonds, which show an interesting transition from a compact cyclic motif leading to the formation of sheet structures (**1a-I**), to a more extended cyclic motif that generates ladder structures (**1a-II**), and to an open-chain motif that forms spiral columnar structures (**1a-III**).

These results will serve as a valuable guide to the rational design of molecular assemblies based on flexible dehydroannulenes, which have been significantly underrepresented in the field of crystal engineering. Here, it would be worth noting again that a four-fold substitution with small, simple groups such as hydroxymethyl can effectively increase the solid-state stability of an otherwise highly unstable system such as the dehydro[24]annulene macrocycle. It is hoped that this contribution will encourage further exploration into the solid-state chemistry of a wide variety of dehydroannulenes and related acetylenic macrocycles, especially of those generally considered "unstable". Along these lines, we will further pursue the topochemical polymerization of dehydroannulenes to achieve the controlled synthesis of novel carbon-rich nanostrutures.

■ ASSOCIATED CONTENT

Supporting Information

The Supporting Information is available free of charge on the ACS Publications website at DOI: 10.1021/jacs.6b01939.

Synthetic procedures, spectroscopic data, computation, and X-ray crystallographic analysis (PDF)
Crystallographic information files (CIF)

■ AUTHOR INFORMATION

Corresponding Author

*rubin@chem.ucla.edu

Present Address

†M.S.: Graduate School of Materials Science, Nara Institute of Science and Technology (NAIST), 8916-5 Takayama-cho, Ikoma, Nara 630-0192, Japan

Notes

The authors declare no competing financial interest.

■ ACKNOWLEDGMENTS

We thank the National Science Foundation for financial support through an International Collaboration grant NSF-CHE-1125054, and for instrumentation grants NSF-CHE-9871332 (X-ray) and NSF-CHE-9974928 (NMR). M.S. thanks Dr. Robert D. Kennedy for valuable discussions.

■ REFERENCES

(1) Kissel, P.; Murray, D. J.; Wulftange, W. J.; Catalano, V. J.; King, B. T. *Nat. Chem.* **2014**, *6*, 774–778.
(2) Kory, M. J.; Wörle, M.; Weber, T.; Payamyar, P.; van de Poll, S. W.; Dshemuchadse, J.; Trapp, N.; Schlüter, A. D. *Nat. Chem.* **2014**, *6*, 779–784.
(3) Colson, J. W.; Dichtel, W. R. *Nat. Chem.* **2013**, *5*, 453–465.
(4) Biradha, K.; Santra, R. *Chem. Soc. Rev.* **2013**, *42*, 950–967.

DOI: 10.1021/jacs.6b01939
J. Am. Chem. Soc. 2016, 138, 5939–5956

(5) Chernick, E. T.; Tykwinski, R. R. *J. Phys. Org. Chem.* **2013**, *26*, 742−749.
(6) Rondeau-Gagné, S.; Morin, J.-F. *Chem. Soc. Rev.* **2014**, *43*, 85−98.
(7) Lauher, J. W.; Fowler, F. W.; Goroff, N. S. *Acc. Chem. Res.* **2008**, *41*, 1215−1229.
(8) Ryno, S. M.; Risko, C.; Brédas, J.-L. *J. Am. Chem. Soc.* **2014**, *136*, 6421−6427.
(9) Idé, J.; Méreau, R.; Ducasse, L.; Castet, F.; Bock, H.; Olivier, Y.; Cornil, J.; Beljonne, D.; D'Avino, G.; Roscioni, O. M.; Muccioli, L.; Zannoni, C. *J. Am. Chem. Soc.* **2014**, *136*, 2911−2920.
(10) Akkerman, H. B.; Mannsfeld, S. C. B.; Kaushik, A. P.; Verploegen, E.; Burnier, L.; Zoombelt, A. P.; Saathoff, J. D.; Hong, S.; Atahan-Evrenk, S.; Liu, X.; Aspuru-Guzik, A.; Toney, M. F.; Clancy, P.; Bao, Z. *J. Am. Chem. Soc.* **2013**, *135*, 11006−11014.
(11) Mei, J.; Diao, Y.; Appleton, A. L.; Fang, L.; Bao, Z. *J. Am. Chem. Soc.* **2013**, *135*, 6724−6746.
(12) Dang, M. T.; Wuest, J. D. *Chem. Soc. Rev.* **2013**, *42*, 9105−9126.
(13) O'Neill, M.; Kelly, S. M. *Adv. Mater.* **2011**, *23*, 566−584.
(14) Liu, H.; Xu, J.; Li, Y.; Li, Y. *Acc. Chem. Res.* **2010**, *43*, 1496−1508.
(15) Pramod, P.; Thomas, K. G.; George, M. V. *Chem. - Asian J.* **2009**, *4*, 806−823.
(16) Zang, L.; Che, Y.; Moore, J. S. *Acc. Chem. Res.* **2008**, *41*, 1596−1608.
(17) Coropceanu, V.; Cornil, J.; da Silva Filho, D. A.; Olivier, Y.; Silbey, R.; Brédas, J.-L. *Chem. Rev.* **2007**, *107*, 926−952.
(18) Desiraju, G. R. *J. Am. Chem. Soc.* **2013**, *135*, 9952−9967.
(19) Suzuki, M.; Comito, A.; Khan, S. I.; Rubin, Y. *Org. Lett.* **2010**, *12*, 2346−2349.
(20) Boese, R.; Matzger, A. J.; Vollhardt, K. P. C. *J. Am. Chem. Soc.* **1997**, *119*, 2052−2053.
(21) Dosa, P. I.; Erben, C.; Iyer, V. S.; Vollhardt, K. P. C.; Wasser, I. M. *J. Am. Chem. Soc.* **1999**, *121*, 10430−10431.
(22) Laskoski, M.; Steffen, W.; Morton, J. G. M.; Smith, M. D.; Bunz, U. H. F. *J. Am. Chem. Soc.* **2002**, *124*, 13814−13818.
(23) Jin, H.; Young, C. N.; Halada, G. P.; Phillips, B. L.; Goroff, N. S. *Angew. Chem., Int. Ed.* **2015**, *54*, 14690−14695.
(24) Diegelmann, S. R.; Tovar, J. D. *Macromol. Rapid Commun.* **2013**, *34*, 1343−1350.
(25) Hsu, T.-J.; Fowler, F. W.; Lauher, J. W. *J. Am. Chem. Soc.* **2012**, *134*, 142−145.
(26) Deschamps, J.; Balog, M.; Boury, B.; Ben Yahia, M.; Filhol, J.-S.; van der Lee, A.; Al Choueiry, A.; Barisien, T.; Legrand, L.; Schott, M.; Dutremez, S. G. *Chem. Mater.* **2010**, *22*, 3961−3982.
(27) van den Heuvel, M.; Prenen, A. M.; Gielen, J. C.; Christianen, P. C. M.; Broer, D. J.; Löwik, D. W. P. M.; van Hest, J. C. M. *J. Am. Chem. Soc.* **2009**, *131*, 15014−15017.
(28) Li, Z.; Fowler, F. W.; Lauher, J. W. *J. Am. Chem. Soc.* **2009**, *131*, 634−643.
(29) Jahnke, E.; Weiss, J.; Neuhaus, S.; Hoheisel, T. N.; Frauenrath, H. *Chem. - Eur. J.* **2009**, *15*, 388−404.
(30) Xu, R.; Schweizer, W. B.; Frauenrath, H. *J. Am. Chem. Soc.* **2008**, *130*, 11437−11445.
(31) Frauenrath, H.; Jahnke, E. *Chem. - Eur. J.* **2008**, *14*, 2942−2955.
(32) Dautel, O. J.; Robitzer, M.; Lère-Porte, J.-P.; Serein-Spirau, F.; Moreau, J. J. E. *J. Am. Chem. Soc.* **2006**, *128*, 16213−16223.
(33) Zhu, L.; Tran, H.; Beyer, F. L.; Walck, S. D.; Li, X.; Ågren, H.; Killops, K. L.; Campos, L. M. *J. Am. Chem. Soc.* **2014**, *136*, 13381−13387.
(34) Xu, W. L.; Smith, M. D.; Krause, J. A.; Greytak, A. B.; Ma, S.; Read, C. M.; Shimizu, L. S. *Cryst. Growth Des.* **2014**, *14*, 993−1002.
(35) Rondeau-Gagné, S.; Néabo, J. R.; Desroches, M.; Larouche, J.; Brisson, J.; Morin, J.-F. *J. Am. Chem. Soc.* **2013**, *135*, 110−113.
(36) Rondeau-Gagné, S.; Néabo, J. R.; Desroches, M.; Levesque, I.; Daigle, M.; Cantin, K.; Morin, J.-F. *Chem. Commun.* **2013**, *49*, 9546−9548.
(37) Nagasawa, J.; Yoshida, M.; Tamaoki, N. *Eur. J. Org. Chem.* **2011**, 2247−2255.
(38) Xu, Y.; Smith, M. D.; Geer, M. F.; Pellechia, P. J.; Brown, J. C.; Wibowo, A. C.; Shimizu, L. S. *J. Am. Chem. Soc.* **2010**, *132*, 5334−5335.
(39) Baughman, R. H.; Biewer, M. C.; Ferraris, J. P.; Lamba, J. S. *Synth. Met.* **2004**, *141*, 87−92.
(40) Banerjie, A.; Lando, J. B.; Yee, K. C.; Baughman, R. H. *J. Polym. Sci., Polym. Phys. Ed.* **1979**, *17*, 655−662.
(41) Baughman, R. H.; Yee, K. C. *J. Polym. Sci., Polym. Chem. Ed.* **1974**, *12*, 2467−2475.
(42) Tahara, K.; Inukai, K.; Hara, N.; Johnson, C. A.; Haley, M. M.; Tobe, Y. *Chem. - Eur. J.* **2010**, *16*, 8319−8328.
(43) Hisaki, I.; Shigemitsu, H.; Sakamoto, Y.; Hasegawa, Y.; Okajima, Y.; Nakano, K.; Tohnai, N.; Miyata, M. *Angew. Chem., Int. Ed.* **2009**, *48*, 5465−5469.
(44) Hisaki, I.; Sakamoto, Y.; Shigemitsu, H.; Tohnai, N.; Miyata, M. *Cryst. Growth Des.* **2009**, *9*, 414−420.
(45) Nishinaga, T.; Nodera, N.; Miyata, Y.; Komatsu, K. *J. Org. Chem.* **2002**, *67*, 6091−6096.
(46) Bunz, U. H. F.; Enkelmann, V. *Chem. - Eur. J.* **1999**, *5*, 263−266.
(47) Haley, M. M.; Bell, M. L.; English, J. J.; Johnson, C. A.; Weakley, T. J. R. *J. Am. Chem. Soc.* **1997**, *119*, 2956−2957.
(48) Zhou, Q.; Carroll, P. J.; Swager, T. M. *J. Org. Chem.* **1994**, *59*, 1294−1301.
(49) Baldwin, K. P.; Matzger, A. J.; Scheiman, D. A.; Tessier, C. A.; Vollhardt, K. P. C.; Youngs, W. J. *Synlett* **1995**, 1215−1218.
(50) Hisaki, I.; Senga, H.; Shigemitsu, H.; Tohnai, N.; Miyata, M. *Chem. - Eur. J.* **2011**, *17*, 14348−14353.
(51) Hisaki, I.; Senga, H.; Sakamoto, Y.; Tsuzuki, S.; Tohnai, N.; Miyata, M. *Chem. - Eur. J.* **2009**, *15*, 13336−13340.
(52) Hisaki, I.; Sakamoto, Y.; Shigemitsu, H.; Tohnai, N.; Miyata, M.; Seki, S.; Saeki, A.; Tagawa, S. *Chem. - Eur. J.* **2008**, *14*, 4178−4187.
(53) Spitler, E. L.; Johnson, C. A.; Haley, M. M. *Chem. Rev.* **2006**, *106*, 5344−5386.
(54) Shetty, A. S.; Zhang, J.; Moore, J. S. *J. Am. Chem. Soc.* **1996**, *118*, 1019−1027.
(55) Sondheimer, F.; McQuilkin, R. M.; Garratt, P. J. *J. Am. Chem. Soc.* **1970**, *92*, 6682−6683.
(56) Curtis, S. M.; Le, N.; Fowler, F. W.; Lauher, J. W. *Cryst. Growth Des.* **2005**, *5*, 2313−2321.
(57) Enkelmann, V.; Graf, H. J. *Acta Crystallogr., Sect. B: Struct. Crystallogr. Cryst. Chem.* **1978**, *34*, 3715−3719.
(58) Steiner, T. *Angew. Chem., Int. Ed.* **2002**, *41*, 48−76.
(59) Venkataraman, D.; Lee, S.; Zhang, J.; Moore, J. S. *Nature* **1994**, *371*, 591−593.
(60) Etter, M. C.; MacDonald, J. C.; Bernstein, J. *Acta Crystallogr., Sect. B: Struct. Sci.* **1990**, *46*, 256−262.
(61) Calculations were performed at the BHandHLYP/6-31G(d) level of theory using Gaussian 09, Revision A.02. See the SI for the full citation of Gaussian 09 and computational details.
(62) The crystal obtained from MeOH/THF has a similar, but slightly smaller distortion within the dehydro[24]annulene framework. The corresponding side-to-side distances are 7.617(2) and 8.100(2) Å.
(63) Scheiner, S. *Hydrogen Bonding: A Theoretical Perspective: A Theoretical Perspective*; Oxford University Press: USA, 1997.
(64) Gilli, G.; Gilli, P. *J. Mol. Struct.* **2000**, *552*, 1−15.
(65) Rubin, Y.; Diederich, F. *J. Am. Chem. Soc.* **1989**, *111*, 6870−6871.
(66) Li, Y.; Rubin, Y.; Diederich, F.; Houk, K. N. *J. Am. Chem. Soc.* **1990**, *112*, 1618−1623.
(67) Yamamoto, K.; Shibutani, M.; Kuroda, S.; Ejiri, M.; Ojima, J. *Tetrahedron Lett.* **1986**, *27*, 975−976.
(68) Hisaki, I.; Sonoda, M.; Tobe, Y. *Eur. J. Org. Chem.* **2006**, 833−847.
(69) Awwadi, F. F.; Willett, R. D.; Peterson, K. A.; Twamley, B. *Chem. - Eur. J.* **2006**, *12*, 8952−8960.
(70) Holmes, B. T.; Deb, P.; Pennington, W. T.; Hanks, T. W. *J. Polym. Res.* **2006**, *13*, 133−144.

DOI: 10.1021/jacs.6b01939
J. Am. Chem. Soc. 2016, 138, 5939−5956

(71) Crihfield, A.; Hartwell, J.; Phelps, D.; Walsh, R. B.; Harris, J. L.; Payne, J. F.; Pennington, W. T.; Hanks, T. W. *Cryst. Growth Des.* **2003**, *3*, 313−320.
(72) Feng, X.; Pisula, W.; Zhi, L.; Takase, M.; Müllen, K. *Angew. Chem., Int. Ed.* **2008**, *47*, 1703−1706.
(73) Guo, L.; Bradshaw, J. D.; Tessier, C. A.; Youngs, W. J. *J. Chem. Soc., Chem. Commun.* **1994**, 243−244.
(74) Hanson, A. W. *Acta Crystallogr., Sect. B: Struct. Crystallogr. Cryst. Chem.* **1975**, *31*, 831−834.
(75) Wilhelm, C.; Boyd, S. A.; Chawda, S.; Fowler, F. W.; Goroff, N. S.; Halada, G. P.; Grey, C. P.; Lauher, J. W.; Luo, L.; Martin, C. D.; Parise, J. B.; Tarabrella, C.; Webb, J. A. *J. Am. Chem. Soc.* **2008**, *130*, 4415−4420.
(76) Ouyang, X.; Fowler, F. W.; Lauher, J. W. *J. Am. Chem. Soc.* **2003**, *125*, 12400−12401.
(77) Hohenstein, E. G.; Sherrill, C. D. *J. Phys. Chem. A* **2009**, *113*, 878−886.
(78) Nguyen, T. L.; Scott, A.; Dinkelmeyer, B.; Fowler, F. W.; Lauher, J. W. *New J. Chem.* **1998**, *22*, 129−135.
(79) Etter, M. C. *Acc. Chem. Res.* **1990**, *23*, 120−126.
(80) Tachibana, H.; Kumai, R.; Hosaka, N.; Tokura, Y. *Chem. Mater.* **2001**, *13*, 155−158.
(81) Wilson, R. B.; Duesler, E. N.; Curtin, D. Y.; Paul, I. C.; Baughman, R. H.; Preziosi, A. F. *J. Am. Chem. Soc.* **1982**, *104*, 509−516.
(82) Sarkar, A.; Okada, S.; Matsuzawa, H.; Matsuda, H.; Nakanishi, H. *J. Mater. Chem.* **2000**, *10*, 819−828.
(83) Patel, G. N.; Duesler, E. N.; Curtin, D. Y.; Paul, I. C. *J. Am. Chem. Soc.* **1980**, *102*, 461−466.
(84) Bertault, M.; Canceill, J.; Collet, A.; Toupet, L. *J. Chem. Soc., Chem. Commun.* **1988**, 163−166.
(85) Hwang, I. H.; Lee, S. J.; Chang, J. Y. *J. Polym. Sci., Part A: Polym. Chem.* **2003**, *41*, 1881−1891.
(86) Greenfield, M. A.; Palmer, L. C.; Vernizzi, G.; de la Cruz, M. O.; Stupp, S. I. *J. Am. Chem. Soc.* **2009**, *131*, 12030−12031.
(87) Fujita, N.; Sakamoto, Y.; Shirakawa, M.; Ojima, M.; Fujii, A.; Ozaki, M.; Shinkai, S. *J. Am. Chem. Soc.* **2007**, *129*, 4134−4135.
(88) Nagasawa, J.; Kudo, M.; Hayashi, S.; Tamaoki, N. *Langmuir* **2004**, *20*, 7907−7916.
(89) Spagnoli, S.; Schott, M.; Johnson, M.; Toupet, L. *Chem. Phys.* **2007**, *333*, 236−245.
(90) Brouty, C.; Spinat, P.; Whuler, A. *Acta Crystallogr., Sect. C: Cryst. Struct. Commun.* **1984**, *40*, 1619−1624.
(91) Whuler, A.; Spinat, P.; Brouty, C. *Acta Crystallogr., Sect. C: Cryst. Struct. Commun.* **1984**, *40*, 693−696.
(92) Naddo, T.; Che, Y.; Zhang, W.; Balakrishnan, K.; Yang, X.; Yen, M.; Zhao, J.; Moore, J. S.; Zang, L. *J. Am. Chem. Soc.* **2007**, *129*, 6978−6979.
(93) Laschat, S.; Baro, A.; Steinke, N.; Giesselmann, F.; Hägele, C.; Scalia, G.; Judele, R.; Kapatsina, E.; Sauer, S.; Schreivogel, A.; Tosoni, M. *Angew. Chem., Int. Ed.* **2007**, *46*, 4832−4887.
(94) Feng, X.; Marcon, V.; Pisula, W.; Hansen, M. R.; Kirkpatrick, J.; Grozema, F.; Andrienko, D.; Kremer, K.; Müllen, K. *Nat. Mater.* **2009**, *8*, 421−426.
(95) An, Z.; Yu, J.; Domercq, B.; Jones, S. C.; Barlow, S.; Kippelen, B.; Marder, S. R. *J. Mater. Chem.* **2009**, *19*, 6688−6698.
(96) Pisula, W.; Zorn, M.; Chang, J. Y.; Müllen, K.; Zentel, R. *Macromol. Rapid Commun.* **2009**, *30*, 1179−1202.
(97) Zhao, K.-Q.; Chen, C.; Monobe, H.; Hu, P.; Wang, B.-Q.; Shimizu, Y. *Chem. Commun.* **2011**, *47*, 6290−6292.
(98) Hayashi, H.; Nihashi, W.; Umeyama, T.; Matano, Y.; Seki, S.; Shimizu, Y.; Imahori, H. *J. Am. Chem. Soc.* **2011**, *133*, 10736−10739.
(99) García-Frutos, E. M.; Pandey, U. K.; Termine, R.; Omenat, A.; Barberá, J.; Serrano, J. L.; Golemme, A.; Gómez-Lor, B. *Angew. Chem., Int. Ed.* **2011**, *50*, 7399−7402.
(100) Zhang, Y.; Hanifi, D.; Alvarez, S.; Antonio, F.; Pun, A.; Klivansky, L. M.; Hexemer, A.; Ma, B.; Liu, Y. *Org. Lett.* **2011**, *13*, 6528−6531.
(101) Shimizu, Y.; Miyake, Y.; Yoshida, H.; Monobe, H.; Cook, M. J.; Fujii, A.; Ozaki, M. *Mol. Cryst. Liq. Cryst.* **2011**, *549*, 127−132.
(102) Ni, H.-L.; Monobe, H.; Hu, P.; Wang, B.-Q.; Shimizu, Y.; Zhao, K.-Q. *Liq. Cryst.* **2013**, *40*, 411−420.
(103) He, B.; Pun, A. B.; Klivansky, L. M.; McGough, A. M.; Ye, Y.; Zhu, J.; Guo, J.; Teat, S. J.; Liu, Y. *Chem. Mater.* **2014**, *26*, 3920−3927.
(104) Delgado, M. C. R.; Kim, E.-G.; Filho, D. A.; Bredas, J.-L. *J. Am. Chem. Soc.* **2010**, *132*, 3375−3387.
(105) Calculations were performed using the molecular ADF program: *ADF2013*, ver. 2013; SCM, Theoretical Chemistry, Vrije Universiteit: Amsterdam, The Netherlands. See the SI for the full citation of ADF and computational details.
(106) Brédas, J. L.; Calbert, J. P.; Filho, D. A.; Cornil, J. *Proc. Natl. Acad. Sci. U. S. A.* **2002**, *99*, 5804−5809.
(107) Solooki, D.; Bradshaw, J. D.; Tessier, C. A.; Youngs, W. J.; See, R. F.; Churchill, M.; Ferrara, J. D. *J. Organomet. Chem.* **1994**, *470*, 231−236.
(108) O'Connor, M. J.; Yelle, R. B.; Zakharov, L. N.; Haley, M. M. *J. Org. Chem.* **2008**, *73*, 4424−4432.

DOI: 10.1021/jacs.6b01939
J. Am. Chem. Soc. 2016, 138, 5939−5956